

RESEARCH

Open Access



# PINK1/TAX1BP1-directed mitophagy attenuates vascular endothelial injury induced by copper oxide nanoparticles

Yinzhen Fan<sup>1†</sup>, Zhenli Cheng<sup>2,3†</sup>, Lejiao Mao<sup>1,8</sup>, Ge Xu<sup>1</sup>, Na Li<sup>1</sup>, Mengling Zhang<sup>4</sup>, Ping Weng<sup>4</sup>, Lijun Zheng<sup>1</sup>, Xiaomei Dong<sup>1</sup>, Siyao Hu<sup>4</sup>, Bin Wang<sup>1</sup>, Xia Qin<sup>5,8</sup>, Xuejun Jiang<sup>6,8</sup>, Chengzhi Chen<sup>7,8</sup>, Jun Zhang<sup>1,8\*</sup>  and Zhen Zou<sup>1,8\*</sup>

## Abstract

Copper oxide nanoparticles (CuONPs) are widely used metal oxide NPs owing to their excellent physical–chemical properties. Circulation translocation of CuONPs after inhalation leads to vascular endothelial injury. Mitochondria, an important regulatory hub for maintaining cell functions, are signaling organelles in responses to NPs-induced injury. However, how mitochondrial dynamics (fission and fusion) and mitophagy (an autophagy process to degrade damaged mitochondria) are elaborately orchestrated to maintain mitochondrial homeostasis in CuONPs-induced vascular endothelial injury is still unclear. In this study, we demonstrated that CuONPs exposure disturbed mitochondrial dynamics through oxidative stress-dependent manner in vascular endothelial cells, as evidenced by the increase of mitochondrial fission and the accumulation of fragmented mitochondria. Inhibition of mitochondrial fission with Mdivi-1 aggravated CuONPs-induced mtROS production and cell death. Furthermore, we found that mitochondrial fission led to the activation of PINK1-mediated mitophagy, and pharmacological inhibition with wortmannin, chloroquine or genetical inhibition with siRNA-mediated knockdown of PINK1 profoundly repressed mitophagy, suggesting that the protective role of mitochondrial fission and PINK1-mediated mitophagy in CuONPs-induced toxicity. Intriguingly, we identified that TAX1BP1 was the primary receptor to link the ubiquitinated mitochondria with autophagosomes, since *TAX1BP1* knockdown elevated mtROS production, decreased mitochondrial clearance and aggravated CuONPs-induced cells death. More importantly, we verified that urolithin A, a mitophagy activator, promoted mtROS clearance and the removal of damaged mitochondria induced by CuONPs exposure both in vitro and in vivo. Overall, our findings indicated that modulating mitophagy may be a therapeutic strategy for pathological vascular endothelial injury caused by NPs exposure.

## Highlights

1. CuONPs disturb mitochondrial dynamics and trigger mitophagy in vascular endothelial cells and mouse blood vessel.

\*Correspondence: zhangjun@cqmu.edu.cn; zouzhen@cqmu.edu.cn

<sup>†</sup>Yinzhen Fan and Zhenli Cheng contributed equally to this work

<sup>1</sup> Molecular Biology Laboratory of Respiratory Disease, Institute of Life Sciences, Chongqing Medical University, Chongqing 400016, People's Republic of China

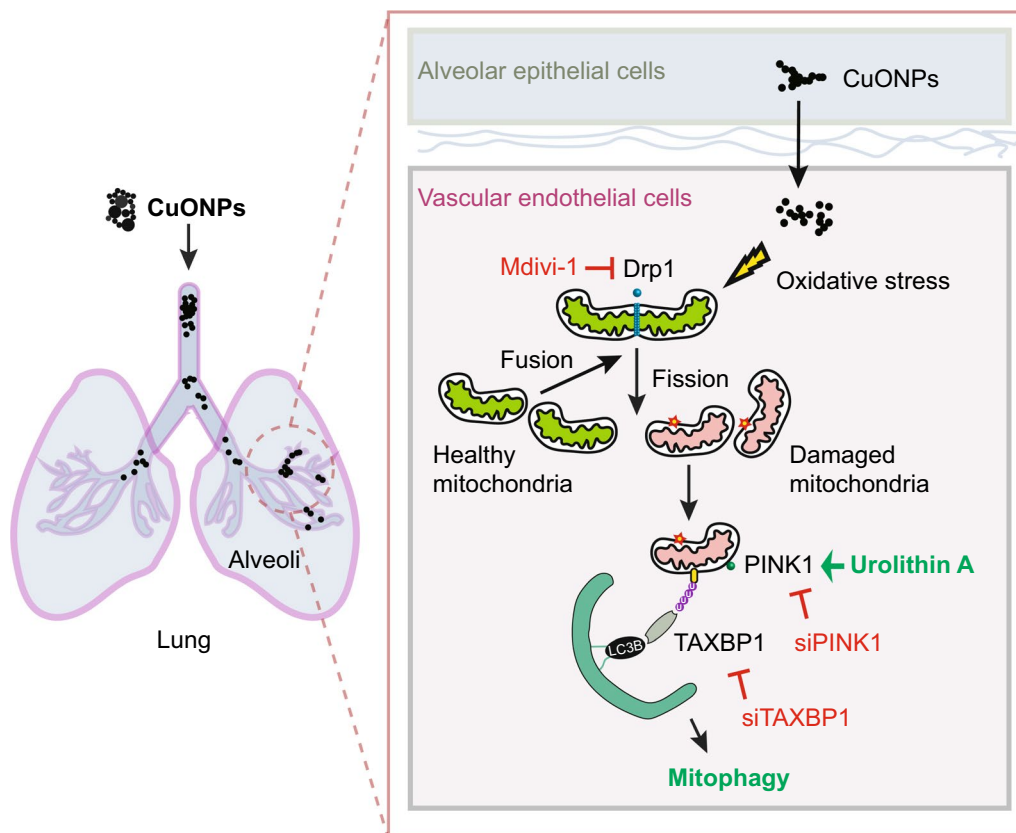
Full list of author information is available at the end of the article



2. PINK1/TAX1BP1-mediated mitophagy regulates the removal of excessive ROS and aberrant mitochondria in CuONPs-treated vascular endothelial cells.
3. The mitophagy activator urolithin A attenuates CuONPs-induced vascular endothelial cells death and mice vascular injury.

**Keywords:** CuONPs, Vascular endothelial injury, Mitophagy, PINK1/TAX1BP1, Urolithin A

**Graphical Abstract**



**Introduction**

Copper oxide nanoparticles (CuONPs) are widely used in industrial and biomedical fields owing to their excellent physical–chemical properties, earth-abundant and inexpensive properties [1]. For example, CuONPs have been efficiently used for biological sensors to detect glucose, cholesterol, disease-related protein biomarkers and others [2]. CuONPs nanomedicines have been used against various types of tumors [3–5]. In addition, CuONPs show excellent antimicrobial activities against *Staphylococcus aureus* and *Escherichia coli* [6]. Currently, CuONPs is also developed as antiviral surface coatings suppressing the spread of SARS-CoV-2 [7–9]. Meanwhile, CuO nanocomposites are designed as a

potential treatment against bacterial infected diabetic non-healing wounds [10, 11].

However, the widespread application of CuONPs in industrial and biomedical fields has seriously threatened the health of this human being. CuONPs are recognized as particularly highly toxic NPs, when compared to many other metal oxide NPs [1, 12]. Accumulating evidence shows that the transformation of nanomaterials in the environment or living systems is closely related to nanomaterials stability and toxicity [13, 14]. CuONPs also undergo chemical transformation under conditions relevant to living systems and the natural environment. CuONPs dissolve at lysosomal pH (4–5) solution and undergo sulfidation by a dissolution-precipitation

mechanism [15]. Consistently, in our previous *in vitro* study, we confirmed that lysosomal deposition of CuONPs facilitated the release of Cu ions from CuONPs-treated vascular endothelial cells [16]. However, the underlying protective mechanisms against CuONPs toxicity are not yet fully understood.

Inhaled NPs are closely linked to cardiovascular diseases [17–19]. Exposure to combustion-derived NPs impairs vascular physiological functions and inhibits arterial vasodilatation both in pre-clinical (rat model) and clinical model [20]. Pulmonary exposure to engineered NPs results in oxidative stress and inflammation, consequently contributes to the progression of atherosclerosis [21–23]. Vascular endothelial cells cover the inner surface of all blood vessels and serve as a regulatory hub of systemic circulation [24]. Because inhaled NPs can translocate into systemic circulation and accumulate at the sites of vascular disease, NPs may directly interact with vascular endothelial cells and impair vascular physiological functions [25].

Mitochondrial dynamics is an important metabolic and regulatory hub characterized by mitochondrial fusion, fission and degradation of damaged mitochondria [26]. Disruption of mitochondrial dynamics leads to multiple diseases such as cancers, cardiovascular disease, neurodegenerative disease, aging and others [27]. We previously reported that CuONPs treatment resulted in mitochondrial dysfunction and excessive mitochondrial ROS (mtROS) production in vascular endothelial cells [16, 28, 29]. Nonetheless, whether the mitochondrial dynamics is involved in CuONPs-induced vascular endothelial injury is still unclear.

Mitophagy is a selective autophagic process that specifically degrading damaged mitochondria by autophagy-lysosome machinery to maintain mitochondrial homeostasis [30, 31]. Mitophagy is regulated by the ubiquitin kinase P<sup>T</sup>EN induced kinase 1 (PINK1) and mitophagy receptors. Several studies have demonstrated mitophagy is involved in nanoparticle-induced cytotoxicity including human fetal hepatocyte line L-02

[32], human hepatocellular carcinoma (HepG2) cells [33, 34], human lung adenocarcinoma (A549) cells [35] and murine microglia cell line (BV-2) [36]. In particular, we previously also reported that mitophagy was activated in CuONPs-treated human umbilical vein endothelial cells (HUVECs) [29]. However, the mechanisms of mitophagy in CuONPs-induced vascular endothelial injury is still not fully understood.

In the current study, we demonstrated the involvement of mitochondrial dynamics and mitophagy in CuONPs exposure-induced vascular endothelial injury *in vitro* and *in vivo*. In addition, we investigated the roles of urolithin A (UA), which is a first-in-class natural compound that inducing mitophagy. This study uncovers the importance of mitophagy-mediated mitochondrial homeostasis in CuONPs-mediated cytotoxicity and highlights the potential application of mitophagy activator in preventing NPs-triggered vascular injury.

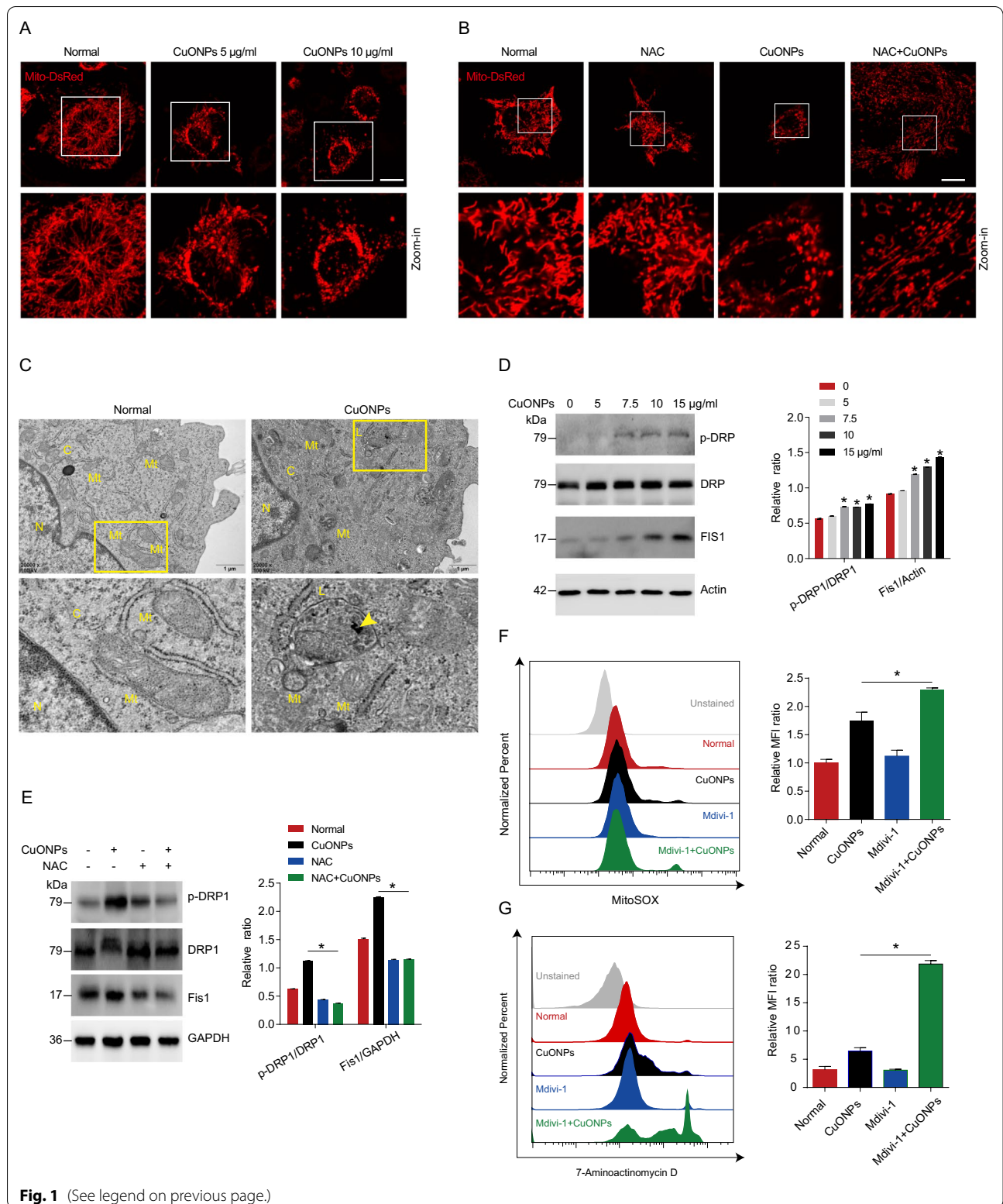
## Results

### CuONPs disturbs mitochondrial dynamics in vascular endothelial cells

Physical properties of CuONPs have been reported in our previous study [16, 37]. Briefly, transmission electron microscopy (TEM) analysis showed that CuONPs were spherical NPs with a diameter size of about 50 nm. The spectra of field emission scanning electron microscope/energy dispersive X-ray spectroscopy (FE/SEM-EDS) showed strong peaks of Cu and O specific peaks. Dynamic light scattering (DLS) analysis showed that the average of hydrodynamic radius and zeta potential in the culture medium were 183.70 nm and –13.17 mV. To investigate whether CuONPs undermine mitochondrial dynamics, we constructed a EA.hy926 vascular endothelial cell line stable expressing Mito-DsRed, which labels mitochondria with DsRed fluorescent signal in live cells (Fig. 1A). Mito-DsRed cells were treated with low- or high-dose of CuONPs (5 µg/ml or 10 µg/ml, respectively) for 12 h and detected under confocal microscope. Live cell imaging showed that CuONPs induced

(See figure on next page.)

**Fig. 1** CuONPs induced disturbance of mitochondrial dynamics. **A** Representative fluorescence images of the stable EA.hy926 cell lines expressing Mito-DsRed after treatment with low or high dose CuONPs (5 and 10 µg/ml, respectively) for 12 h. Scale bars, 20 µm. **B** Representative fluorescence images of Mito-DsRed cells which were pretreated with NAC (10 mM) and then treated with CuONPs (10 µg/ml). Scale bars, 20 µm. **C** Representative TEM images of EA.hy926 cells after treatment with CuONPs for 12 h. N, nucleus; C, cytoplasm; Mt, mitochondria; L, lysosomes. Yellow arrow indicates uptaken CuONPs. **D** Western blotting analysis and quantification of the protein levels of p-DRP1, DRP and Fis1 in EA.hy926 treated with 0, 5, 7.5, 10 and 15 µg/ml CuONPs for 12 h, respectively. Actin was served as internal control. **E** Western blotting analysis and quantification of the protein levels of p-DRP1, DRP and Fis1 in EA.hy926 treated with NAC (10 mM) and CuONPs (10 µg/ml). GAPDH was used as internal control. **F** Representative FCM results of EA.hy926 cells after MitoSOX staining. The cells were pretreated with or without Mdivi-1 (25 µM) for 1 h, and then were treated with CuONPs (10 µg/ml) for 12 h. MFI, mean fluorescence intensity. **G** Representative FCM results of EA.hy926 cells after 7-Aminoactinomycin D (7-AAD) staining. In **D**, two-tailed unpaired Student's *t* test was performed for statistical analysis. In **E**, **F** and **G**, one-way ANOVA with Tukey's test was used for multiple comparisons. Results are representative of at least three independent experiments. Data are mean ± S.D. \**p* < 0.05



abnormal changes in mitochondrial morphology characterized by accumulation of fragmented (short tubes) mitochondria in CuONPs-treated cells, indicating that CuONPs treatment promotes mitochondrial fission in vascular endothelial cells (Fig. 1A). Moreover, we showed that N-Acetyl-L-cysteine (NAC), a scavenger of ROS, obviously prevented CuONPs-induced mitochondrial fission, suggesting ROS is an up-stream regulator regulating mitochondrial fission in CuONPs-treated vascular endothelial cells (Fig. 1B). Additionally, TEM images showed that CuONPs indeed damaged mitochondrial dynamics characterized by accumulation of fragmented mitochondria in cells (Fig. 1C). Mitochondrial fission is regulated by a dynamin superfamily of GTPases dynamin related protein 1 (Drp1) and fission protein 1 (Fis1) [38], therefore we analyzed changes in phospho-Drp1 (Drp1 activation form) and Fis1 levels in CuONPs-treated cells via western blotting. The results showed that p-Drp1 (Ser616) and Fis1 were upregulated in CuONPs-treated cells, suggesting that CuONPs induce mitochondrial fission in vascular endothelial cells (Fig. 1D). Moreover, we showed that NAC obviously prevented upregulation of p-Drp1 (Ser616) and Fis1 induced by CuONPs in EA.hy926 cells (Fig. 1E). We then investigated the roles of mitochondrial fission in CuONPs-induced cytotoxicity. Flow cytometry (FCM) results showed that Mdivi-1, a mitochondrial fission inhibitor, significantly exacerbated CuONPs-induced mtROS production in vascular endothelial cells (Fig. 1F). Importantly, Mdivi-1 aggravated CuONPs-induced cell death in EA.hy926 cells (Fig. 1G). Taken together, these results reveal that CuONPs cause mitochondrial dysfunctions and induce mitochondrial fission. Furthermore, mitochondrial fission exerts protective roles in CuONPs-treated vascular endothelial cells.

#### Mitophagy contributes to clearance fragmented mitochondria in CuONPs-treated vascular endothelial cells

Mitophagy is a finely regulated process that maintains cellular homeostasis through clearing dysfunctional mitochondria and excessive mtROS in cells [39]. Previous studies have showed that mitochondrial fission acts

as a trigger of mitophagy process [40–42]. To determine whether mitophagy is triggered in CuONPs-treated EA.hy926 cells, we constructed a GFP-LC3 stable cell line which labels autophagosome with green fluorescent probe. Fluorescence images showed that CuONPs treatment led to more co-localization of GFP-LC3 and mitochondrial protein ATP5B (Fig. 2A), suggesting mitophagy was activated. Interestingly, both autophagy marker LC3B and mitochondria related markers (VDAC1, TIM23 and ATP5B) were upregulated by CuONPs, indicating that CuONPs induce fragmented mitochondria accumulation in vascular endothelial cells (Fig. 2B, C). To determine whether mitophagy mediates clearance of fragmented mitochondria, we pretreated EA.hy926 cells with autophagy inhibitor wortmannin and found it significantly increased protein levels of mitochondria related markers VDAC1, TIM23 and ATP5B (Fig. 2D). FCM results showed that another autophagy inhibitor chloroquine caused more fragmented mitochondria accumulation in CuONPs-treated EA.hy926 cells (Fig. 2E). Thus, mitophagy facilitates removal of damaged mitochondria in CuONPs-treated vascular endothelial cells.

#### CuONPs triggers PINK1-dependent mitophagy in vascular endothelial cells

The ubiquitin kinase PTEN-induced kinase 1 (PINK1) is shown to recruit autophagy receptors to trigger mitophagy [31, 43]. Next, we assessed whether PINK1 mediates the activation of mitophagy and clearance of damaged mitochondria in CuONPs-treated EA.hy926 cells. Western blotting results demonstrated that CuONPs increased PINK1 protein level and the phosphorylation of ubiquitin (a downstream target of PINK1 kinase) in EA.hy926 cells (Fig. 3A). Then, we constructed a EA.hy926 cell line stable co-expressing PINK1-GFP and Mito-DsRed. The results showed that CuONPs recruited PINK1-GFP to Mito-DsRed (labeling mitochondria) (Fig. 3B), suggesting that CuONPs trigger PINK1-dependent mitophagy. To determine the roles of PINK1 in CuONPs-induced cytotoxicity, we knocked down *PINK1* expression in EA.hy926 cells using specific small interfering RNAs (siRNAs) (Fig. 3C). FCM results

(See figure on next page.)

**Fig. 2** Mitophagy facilitates removal of damaged mitochondria in CuONPs-treated cells. **A** Representative immunofluorescence images of colocalization of GFP-LC3 and ATP5B in EA.hy926 cells treated with CuONPs (10  $\mu\text{g}/\text{ml}$ ). White arrows indicate colocalized dots of mitochondrial marker ATP5B with autophagosome marker GFP-LC3. Scale bars, 20  $\mu\text{m}$ . **B** Western blotting analysis and quantification of protein level of LC3B, VDAC1, TIM23 and ATP5B in EA.hy926 treated with CuONPs (0, 5, 10, 15 and 20  $\mu\text{g}/\text{ml}$ , respectively) for 12 h. **C** Western blotting analysis and quantification of protein level of LC3B, VDAC1, TIM23 and ATP5B in EA.hy926 treated with 10  $\mu\text{g}/\text{ml}$  CuONPs for 0, 3, 6, 9 or 12 h. In (B) and (C), two-tailed unpaired Student's *t* test was performed for statistical analysis. GAPDH was used as internal control. **D** The protein expression levels of VDAC1, TIM23 and ATP5B in EA.hy926 treated with or without wortmannin (Wort). Actin was used as internal control. **E** Representative FCM results of EA.hy926 cells labeled with MitoTracker Green FM. The cells were pretreated with or without chloroquine (CQ) for 1 h and then treated 10  $\mu\text{g}/\text{ml}$  CuONPs for 12 h. MFI, mean fluorescence intensity. In **D** and **E**, one-way ANOVA with Tukey's test was used for statistical analysis. All data are representative of at least three independent experiments. Data are mean  $\pm$  S.D. \**p* < 0.05

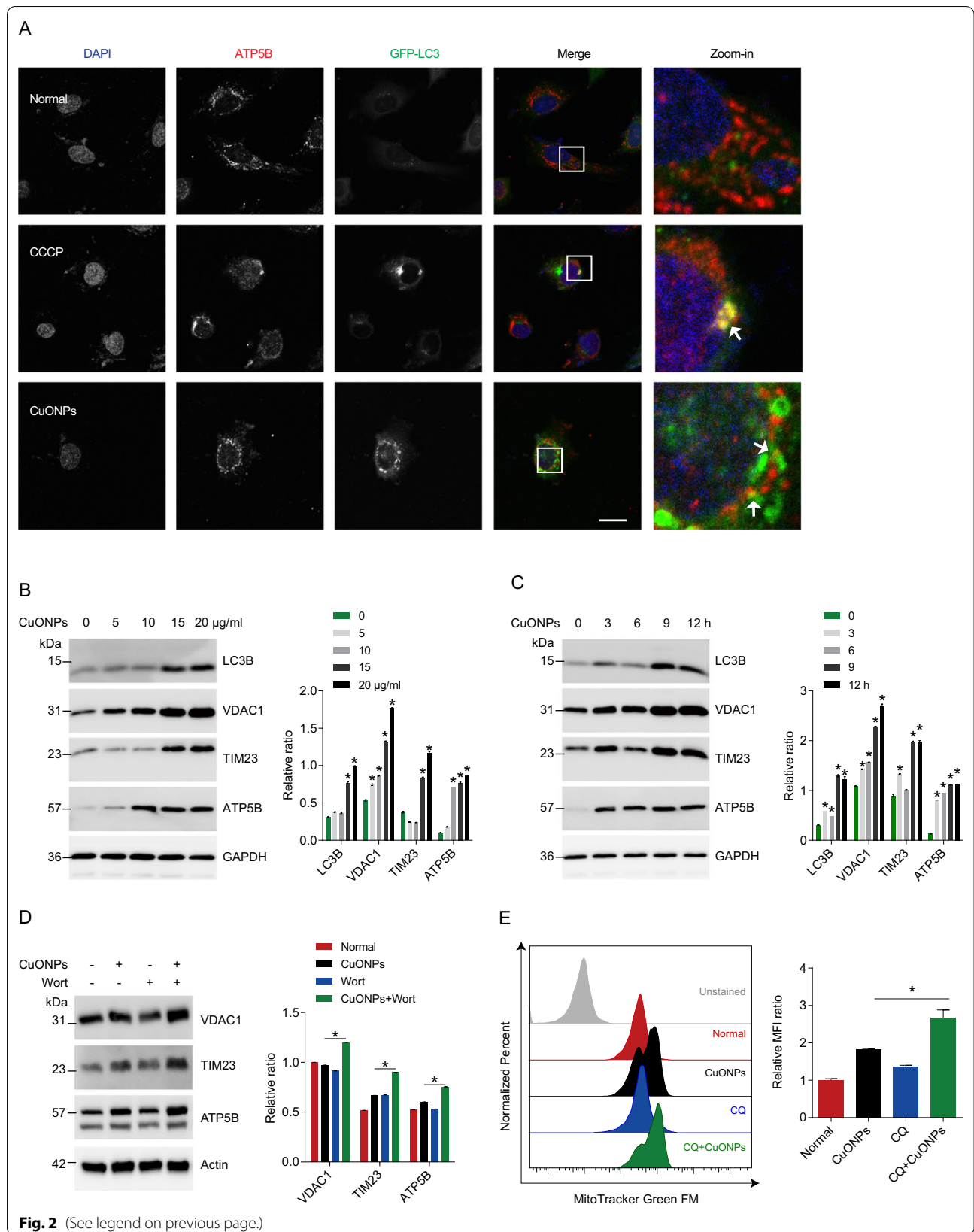
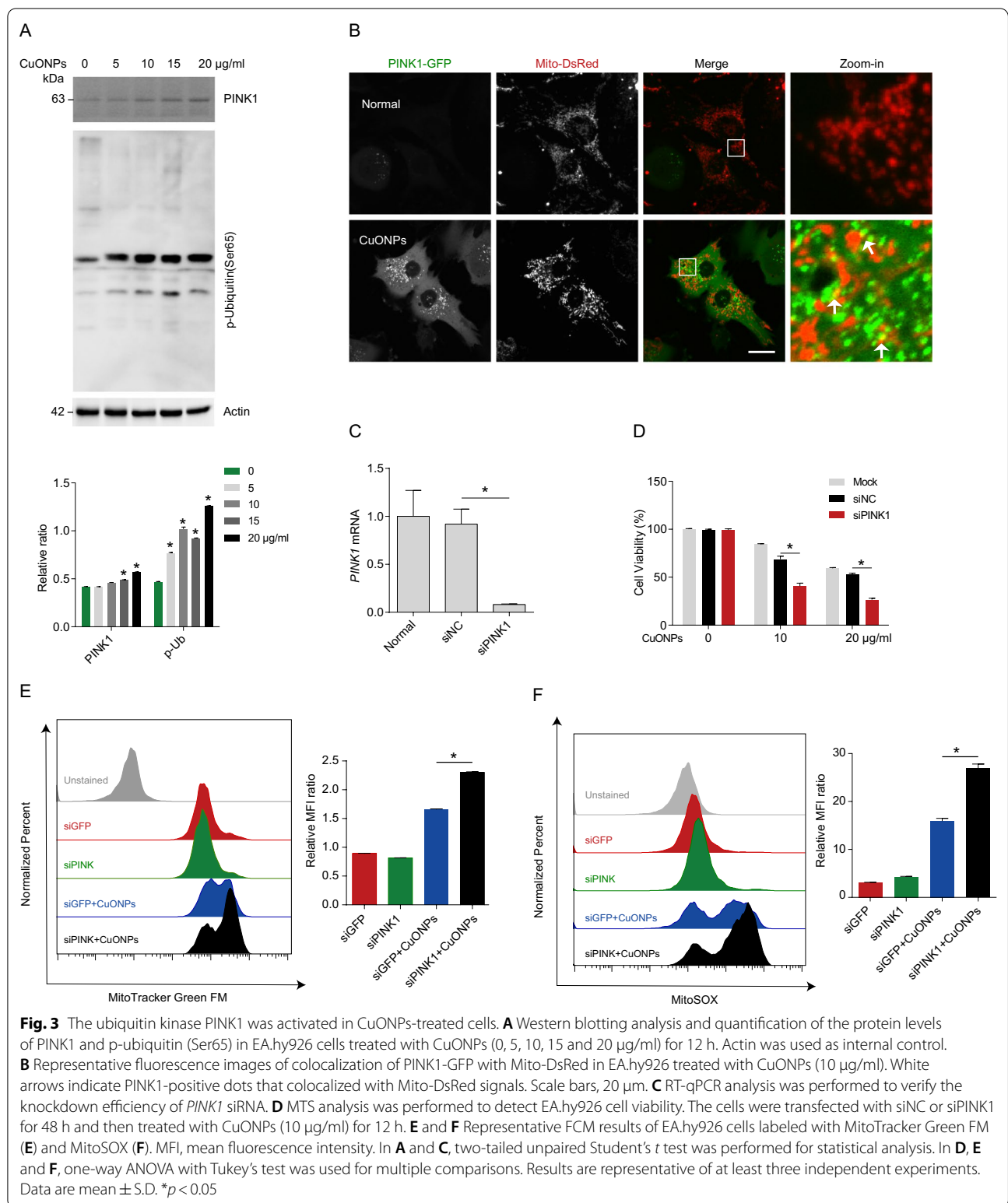


**Fig. 2** (See legend on previous page.)



showed that *PINK1* knockdown increased CuONPs-induced accumulation of damaged mitochondria and mtROS in EA.hy926 (Fig. 3E, F). Furthermore, we found that *PINK1* knockdown exacerbated CuONPs-induced cell death in EA.hy926 (Fig. 3D). Our data thus support that PINK1-dependent mitophagy facilitates clearance of damaged mitochondria in CuONPs-treated EA.hy926 and protects against CuONPs-induced cell death in EA.hy926.

**TAX1BP1 serves as a major mitophagy receptor in CuONPs-treated vascular endothelial cells**

Because mitophagy requires autophagy receptors to linking ubiquitinated mitochondria with autophagosomes

[44, 45]. To determine which receptor mediates removal of damaged mitochondria in CuONPs-treated vascular endothelial cells, we designed siRNAs specific targeting receptor genes including *TAX1BP1*, *NBR1*, *p62*, *OPTN* and *NDP52* respectively. Cell viability results showed that *TAX1BP1* knockdown caused more cell death than other receptor genes in CuONPs-treated EA.hy926 cells, suggesting that TAX1BP1 is the primary receptor mediating removal of damaged mitochondria induced by CuONPs (Fig. 4A). Then, we labeled mitochondria and autophagosomes using Mito-DsRed and GFP-LC3, respectively. Immunofluorescence assay showed that CuONPs treatment induced co-localization of TAX1BP1 with Mito-DsRed and GFP-LC3, indicating that CuONPs recruited

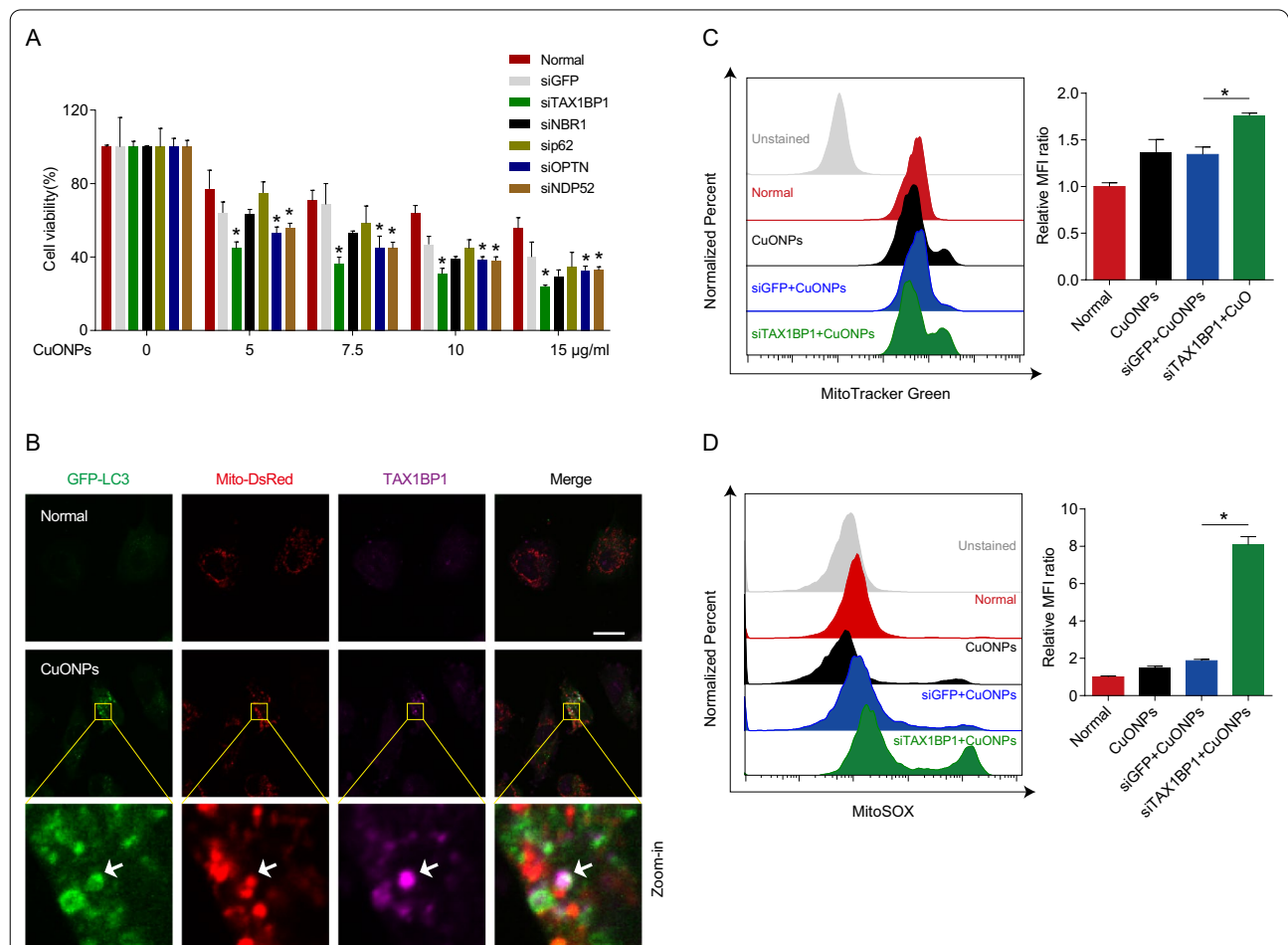


**Fig. 4** TAX1BP1 was the major receptor of CuONPs-induced mitophagy in vascular endothelial cells. **A** MTS analysis was performed to detect EA.hy926 cell viability. Cells were transfected with siNC, siGFP, siTAX1BP1, siNBR1, sip62, siOPTN or siNDP52 for 48 h, and then treated with CuONPs (0, 5, 7.5, 10 and 15 µg/ml) for 24 h. **B** Representative immunofluorescence images indicates colocalization of TAX1BP1 with GFP-LC3 and Mito-DsRed dots in EA.hy926 stable cell line expressing GFP-LC3 and Mito-DsRed after treatment with 10 µg/ml CuONPs for 12 h. White arrow indicate TAX1BP1-positive dots that colocalized with GFP-LC3 and Mito-DsRed signals. Scale bars, 20 µm. **C** and **D** Representative FCM results of EA.hy926 cells labeled with MitoTracker Green FM (**C**) and MitoSOX (**D**), respectively. The cells were transfected with siNC or siTAX1BP1 for 48 h and then treated with CuONPs (10 µg/ml) for 12 h. All data were statistically analyzed using one-way ANOVA with Tukey’s test. Results are representative of at least three independent experiments. Data are mean ± S.D. \**p* < 0.05

TAX1BP1 to mitophagosomes in EA.hy926 cells (Fig. 4B). To further determine the function of TAX1BP1 during mitophagy, we detected mitochondria mass and mtROS level in *TAX1BP1* knockdown cells. FCM results showed that *TAX1BP1* knockdown inhibited mitophagy-mediated removal of damaged mitochondria, resulting in more mitochondria accumulation in CuONPs-treated EA.hy926 cells (Fig. 4D). Moreover, *TAX1BP1* knockdown induced more mtROS accumulation in CuONPs-treated EA.hy926 cells (Fig. 4C). This suggests TAX1BP1 is necessary for CuONPs-mediated mitophagy in vascular endothelial cells.

#### Urolithin A induces PINK1-dependent mitophagy and rescues CuONPs-induced vascular endothelial cell death

Urolithin A (UA) is a gut microbiome-derived natural product derived from ingested ellagitannins and ellagic acid by gut bacteria [46]. Previous studies have shown that UA induces mitophagy and alleviates a variety of diseases such as aging-related diseases [47], neurodegeneration diseases [48, 49] and muscular dystrophy [50]. To determine whether UA protects against CuONPs-induced cytotoxicity, we firstly analyzed mitophagy flux in UA-treated EA.hy926 cells. In Mito-DsRed/GFP-LC3 stable cell line, the co-localization of Mito-DsRed (mitochondria) and GFP-LC3 (autophagosomes) revealed that mitophagy was activated in CuONPs- or UA-treated cells. (Fig. 5A). Moreover, UA pretreatment upregulated CuONPs-induced mitophagy level in EA.hy926 (Fig. 5A). FCM and western blotting results showed that UA facilitated removal of damaged mitochondria in CuONPs-treated EA.hy926 cells (Fig. 5C, D). Consistently, UA promoted mtROS clearance in CuONPs-treated cells (Fig. 5E). Then, we investigated the role of PINK1 in UA-treated EA.hy926 cells and the results showed that UA promoted PINK1-GFP recruitment to mitochondria (Fig. 5B). The results also revealed that UA reduced CuONPs-induced cell death in EA.hy926 cells, while *PINK1* knockdown eliminated protective effect of UA against CuONPs-induced cell death (Fig. 5F). These data suggest UA triggers PINK1-dependent mitophagy and

protects against CuONPs-induced vascular endothelial cell death.

#### Urolithin A alleviates CuONPs-induced vascular injury in mice.

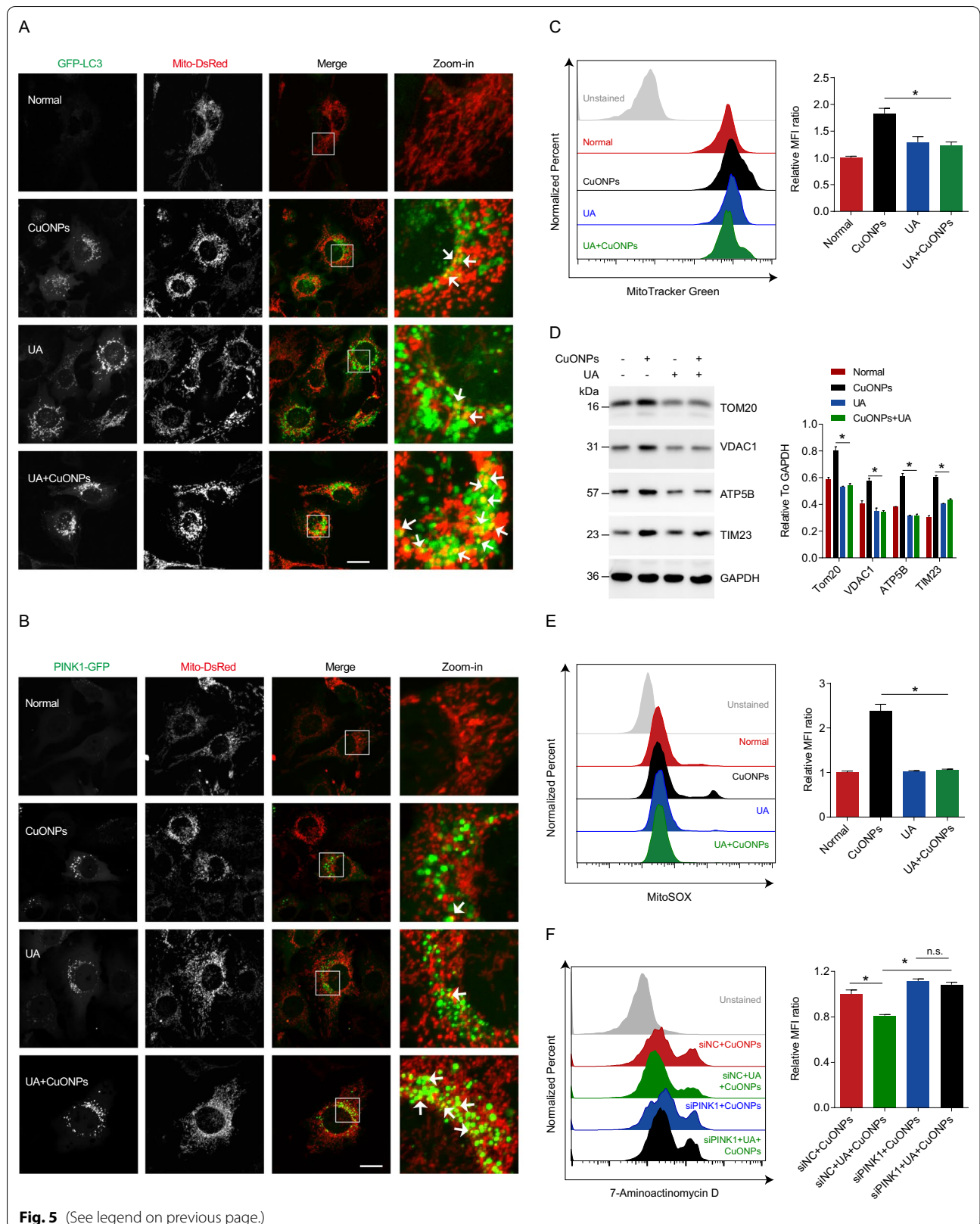
To determine the protective role of UA against vascular injury in CuONPs-treated mice, we established CuONPs pulmonary exposure mouse model as described in our previous study [37]. The mice experimental design was illustrated in the Fig. 6A. Through ultrastructural observation under TEM, we showed that CuONPs pulmonary exposure resulted in accumulation of damaged or fragmented mitochondria in mouse aortic endothelial cells (Fig. 6B). Western blotting results revealed that CuONPs increased protein levels of mitochondria fission marker Fis1 and mitochondria related proteins TIM23 and ATP5B in mouse aortic vessels (Fig. 6C, D). Meanwhile, LC3B was upregulated in CuONPs exposure group, indicating CuONPs indeed activated mitophagy flux in mouse aortic vessels (Fig. 6D). Next, we showed that UA obviously alleviated CuONPs-induced mitochondrial dysfunctions (characterized by cristae rarefaction and swelling) in vascular endothelial cells (Fig. 6E). Moreover, western blotting results demonstrated that UA significantly decreased TIM23, ATP5B and VDAC1 protein level in aortic vessels of CuONPs-treated mice, indicating that UA accelerated removal of damaged mitochondria in mouse aortic vessels induced by CuONPs exposure (Fig. 6F). Finally, we showed that UA alleviated CuONPs-induced oxidative stress in mouse aortic vessels (Fig. 6G). These data indicate UA induces mitophagy and ameliorates NPs exposure-induced vascular injury.

#### Discussions

Mitochondria participate in various aspects of cellular metabolisms, including energy metabolism, biosynthetic hubs, mtROS balance and cellular waste management [51]. Mitochondrial dysfunctions trigger many metabolic diseases, such as cardiomyopathy, respiratory failure, liver failure, diabetes mellitus and neurological disease [27, 52]. It is widely accepted that mitochondrial

(See figure on next page.)

**Fig. 5** UA alleviated CuONPs-induced cell death. **A** Representative fluorescence images of EA.hy926 cell line stable expressing GFP-LC3 and Mito-DsRed. **B** Representative fluorescence images of EA.hy926 cell line stable expressing PINK1-GFP and Mito-DsRed. In **A** and **B**, the cells were treated with UA (100  $\mu$ M), CuONPs (10  $\mu$ g/ml) and UA + CuONPs for 12 h, respectively. White arrows indicate PINK1-positive or LC3-positive dots that colocalized with damaged mitochondria signals. Scale bars, 20  $\mu$ m. **C** Representative FCM results of EA.hy926 staining with mitochondrial mass marker MitoTracker Green FM. MFI, mean fluorescence intensity. **D** Western blotting analysis and quantification of protein levels of TOM20, VDAC1, ATP5B and TIM23 in CuONPs-treated EA.hy926 cells with or without UA. **E** Representative FCM results of EA.hy926 staining with mtROS probe MitoSOX. **F** Representative FCM results of EA.hy926 staining with 7-AAD. EA.hy926 cells were transfected with siNC or siPINK1 for 48 h, and then treated with UA (100  $\mu$ M) and CuONPs (10  $\mu$ g/ml) for 24 h. n.s., not significance. The cells were treated with CuONPs (10  $\mu$ g/ml) or UA + CuONPs for 12 h, respectively. All data were statistically analyzed using One-way ANOVA with Tukey's test. The results are representative of at least three independent experiments. Data are mean  $\pm$  S.D. \* $p$  < 0.05



dysfunctions and mtROS imbalance are main causes of CuONPs-induced cellular toxicity (Table 1). Recently, a study reported that CuONPs was a solid source of oxygen, which directly captured electrons from the respiratory chain and harnessed the trapped electrons for ROS generation. This finding proposed that CuONPs can disturb mitochondrial respiratory, damage cellular energy supply and simultaneously induce mtROS-mediated oxidative stress [53].

Mammalian cells have evolved several mechanisms for maintaining mitochondrial homeostasis, such as mitochondrial fission–fusion dynamics [54]. Mitochondrial fission is involved in mitochondria biogenesis and mitochondria quality control by promoting elimination of damaged mitochondria. Mitochondrial fusion participates in cellular stress response through rescuing non-functional mitochondria [38, 46, 55]. Mitochondrial dynamics imbalance was involved in multiple NPs-induced toxicity [32, 33, 56]. In this study, we demonstrated that CuONPs exposure caused oxidative stress and consequently induced mitochondria fission in vascular endothelial cells characterized by increases of fission mediators Fis1 and p-Drp1 (Fig. 1A, B, D, E). It is well documented that excessive mtROS-mediated mitochondrial stress contributes to mitochondria fission [54]. Mitochondrial superoxide anions ( $O_2^{\cdot-}$ ) is the major form of mtROS. We previously reported that CuONPs exposure resulted in accumulation of mitochondrial  $O_2^{\cdot-}$  in vascular endothelial cells [28, 29]. Consequently, excessive mitochondrial  $O_2^{\cdot-}$  triggered oxidative DNA damage and p38 MAPK-dependent vascular endothelial cells death [57]. In this study, we further revealed that mitochondrial  $O_2^{\cdot-}$  was involved in CuONPs-induced mitochondrial fission in that ROS scavenger NAC decreased p-DRP1 and Fis1 and significantly inhibited CuONPs-induced mitochondrial fission (Fig. 1B, E). Consistently, mitochondrial  $O_2^{\cdot-}$  promotes mitochondrial fission in coronary endothelial cells, while  $O_2^{\cdot-}$  scavenger TEMPOL significantly inhibits mitochondrial fission

in Diabetic mice [58]. In ischemia/reperfusion (I/R) cell model, I/R-induced mitochondrial fission is also obviously inhibited by  $O_2^{\cdot-}$  scavenger [59]. All these results indicate mitochondrial  $O_2^{\cdot-}$  functions as an up-stream signal of mitochondrial fission.

Currently, mitochondrial fission contributes to pro-survival or pro-death in cells under oxidative stress is still controversial. An early study demonstrated that inhibition of mitochondrial fission prevented high glucose-induced cardiomyocytes apoptosis [60]. Clare Sheridan et al. reported that mitochondrial fission induced by pro-apoptotic BCL2-associated X protein (BAX) and the release of pro-death cytochrome *c* were two separable events [61]. In contrast with these findings, a recent study reported that anti-apoptotic protein Myeloid cell leukemia 1 (MCL-1) induced mitochondrial fission and inhibit cardiomyocytes death, suggesting that mitochondrial fission protects against stress-induced cell death [62]. Masahiro Morita et al. recently found that nutrient-sensing regulator mTOR complex 1 (mTORC1) regulated mitochondrial dynamics, and mTOR inhibitor prevented mitochondrial fission and consequently triggered apoptosis [63]. Accordingly, mitochondrial fission may be bad or good and therefore plays dual roles in different physiological context. In this study, we found that mitochondrial fission inhibitor Mdivi-1 aggravated CuONPs-induced oxidative stress and cells death in EA.hy926 (Fig. 1F, G). This indicates that mitochondrial fission is a crucial pro-survival process in CuONPs-induced cytotoxicity.

Accumulating evidence has highlighted that mitochondrial fission contributes to removal of damaged mitochondria via autophagy (a process termed as mitophagy) [64–66], through which protects against many types of NPs-induced cytotoxicity [34–36, 67]. Mitophagy is regulated by ubiquitin kinase PTEN induced kinase 1 (PINK1) and mitophagy receptors including Tax1 binding protein 1 (TAX1BP1), Calcium binding and coiled-coil domain 2 (CALCOCO2, NDP52), Optineurin (OPTN), Neighbor of BRCA1 gene 1 protein (NBR1) or Sequestosome-1

(See figure on next page.)

**Fig. 6** UA alleviated CuONPs-induced vascular injury in mice. **A** Schematic figure for animal experiments. C57BL/6 J mice were treated with vehicle (PBS) or UA (30 mg/kg) for 1 week by intragastric gavage (i.g.), and then exposed to CuONPs via intratracheal instillation (i.t.), meanwhile the mice in UA group and CuONPs + UA group were continuously treated with UA (30 mg/kg) by gavage for 3 days. **B** Representative TEM images of mice abdominal aorta dissected from CuONPs-treated mice. Mice were intratracheally instilled with CuONPs (5 mg/kg) for 3 days. N, nucleus; C, cytoplasm; Mt, mitochondria; IEM, internal elastic membrane. **C** and **D** Western blotting analysis and quantification of protein levels of Fis1, TIM23, ATP5B and LC3B in mice aorta tissues. Mice were intratracheally instilled with 2.5 mg/kg or 5 mg/kg CuONPs for 3 days. Actin was used as the internal control. **E** Representative TEM images of mice abdominal aorta dissected from CuONPs-treated mice. Mice were treated with UA (30 mg/kg) for 10 days by intragastric gavage and then intratracheally instilled with CuONPs (5 mg/kg) at day 7. N, nucleus; C, cytoplasm; Mt, mitochondria; IEM, internal elastic membrane. **F** Western blotting analysis and quantification of protein levels of mitochondria related proteins in aorta tissues dissected from CuONPs-treated mice with or without UA. Actin was used as the internal control. **G** Western blotting analysis and quantification of protein levels of oxidative stress response proteins in aorta tissues dissected from CuONPs-treated mice with or without UA. Actin was used as the internal control. In **C** and **D**, two-tailed unpaired Student's *t* test was performed for statistical analysis. In **F** and **G**, one-way ANOVA with Tukey's test was used for multiple comparisons. Results are representative of at least three independent experiments. Data are mean  $\pm$  S.D. \**p* < 0.05

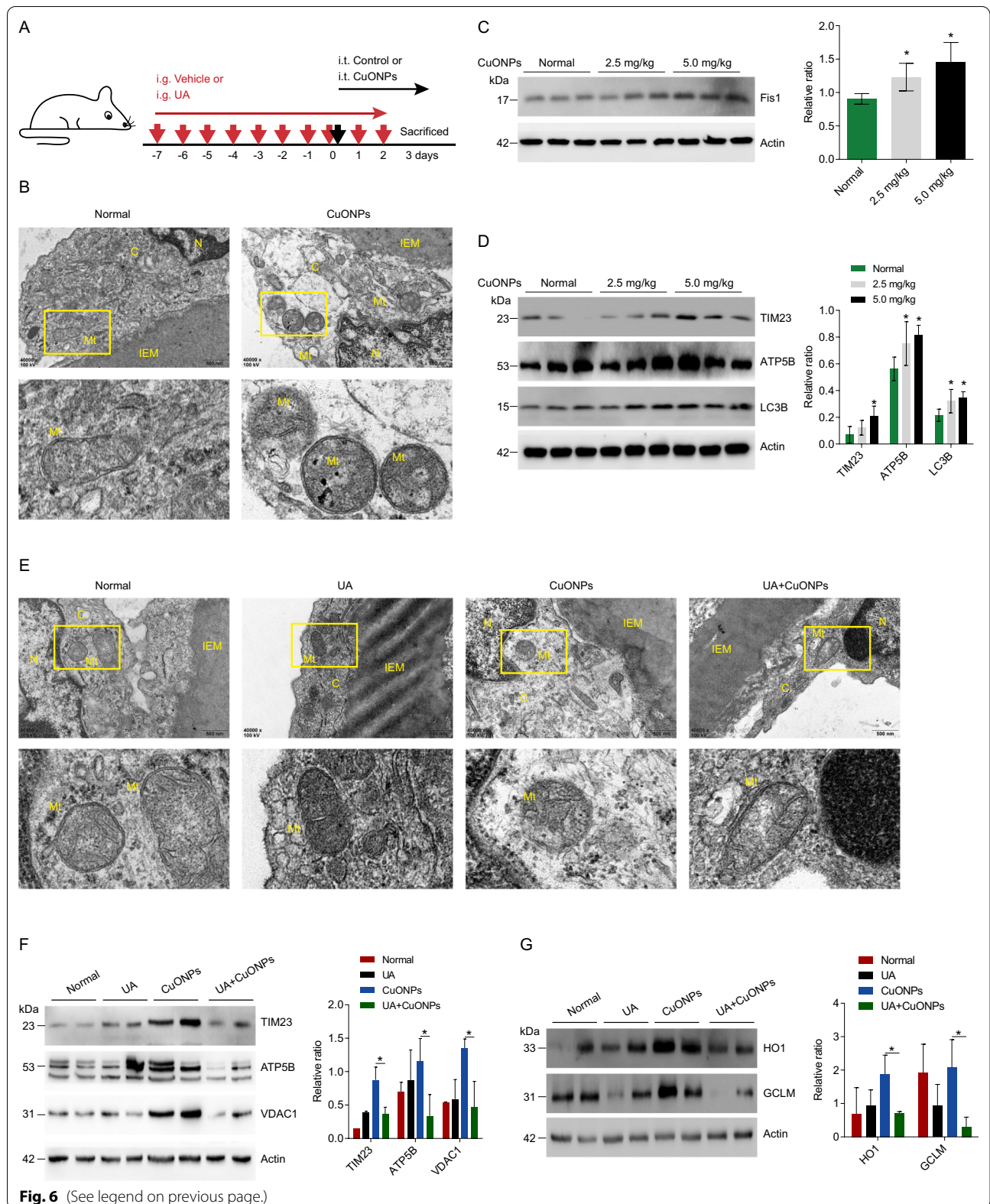


**Table 1** Toxic effects and mechanisms of CuONPs

Nanoparticle source	Particle size	Dose	Exposure time	Cell line/in vivo models	Mechanism of toxicity	References (DOI)
Sigma-Aldrich	< 50 nm	100 mg/kg body weight (intraperitoneal instillation)	14 d	Wistar male rats	Oxidative stress, DNA damage and apoptosis in liver	10.1038/s41598-020-67784-y
Self-synthesized		0, 1.25, 2.5, 5, 10 and 20 µg/ml	48, 72 h	Renal cell carcinoma (786O, A498, CAKI-1, SR786O and HK-2)	ER stress; Apoptosis	10.1016/j.biomaterials.2017.09.008
Sigma-Aldrich	< 50 nm	0–80 µg/ml	4, 24 h	Rat small intestine epithelial cells (IEC-6) 3D human small intestinal tissue model (EpiIntestinal)	ROS production; Cytotoxicity	10.1080/17435390.2019.1578428
Sigma-Aldrich	20–40 nm	10 µg/g body weight (intranasal perfusion)	60 d	Rat liver cells (BRL 3A); Wistar male rats	Oxidative stress, ER stress and apoptosis in liver	10.1016/j.jhazmat.2020.123349
Self-synthesized	141 ± 13 nm in water	0, 10, 100, 1000 µM	5 h	Rat glioma cell line (C6)	ROS production; Cytotoxicity	10.1007/s11064-016-2020-z
Self-synthesized	75 nm	0, 1.25, 2.5 and 5 µg/ml	24 h	Primary human umbilical vein endothelial cells (HUVECs)	Impairment of angiogenesis	10.1039/c3nr04363k
Sigma-Aldrich	< 50 nm	0, 5, 10, 15 and 20 µg/ml	12 h	Murine macrophage J774A.1	Lysosomal damage; Oxidative stress; Inflammation	10.1016/j.jhazmat.2021.125134
Self-synthesized		15.63–625 µM	24 h	Mouse fibroblasts (L929)	DNA damage; ROS production	10.1016/j.tiv.2021.105252
Sigma-Aldrich	< 50 nm	1.25, 2.5 or 5 mg/kg (intratracheal instillation)	3 d	Male C57BL/6 mice	Oxidative stress; Autophagy dysfunction; Acute lung injury	10.1186/s12951-021-00909-1
Ionic Liquidess Technologies	15–100 nm	0–240 µg/ml	18 h	Leukemic cell line (HL60)	Mitochondrial damage; ROS production; DNA damage	10.1016/j.tiv.2015.05.020
Sigma-Aldrich	< 50 nm	0, 10, 20, and 40 µg/ml	0, 1, 3, 6, 12 h	Human umbilical vein endothelial cells (HUVECs)	Lysosomal impairment; ROS production; DNA damage	10.2147/JIN.S241157 10.1016/j.ifs.2020.117571 10.1016/j.freeradbiomed.2018.09.032 10.1016/j.biomaterials.2018.01.048
Sigma-Aldrich	< 50 nm	0, 5, 10, 15, 20 µg/ml (in vitro); 2.5–5.0 mg/kg (intratracheal instillation)	12 h 3 d	Human umbilical vein endothelial cell line (EA.hy926); Male C57BL/6 mice	Mitochondrial dysfunctions; mtROS production; Vascular injury	This study
Sigma-Aldrich		0, 0.01, 0.1, 1, 10, 100 µM	48 h	Human SH-SY5Y neuroblastoma cells (CRL-2266) Human neuroglioma H4 (HTB-148) Rat PC12 (CRL-1721)	ROS production; Apoptosis	10.3390/ijerph17031005
Self-synthesized	124 nm	10 µg/ml	24 h	Human pancreatic cancer cell line (PANC1)	Mitochondrial dysfunctions; ROS production; Apoptosis	10.1038/s41598-019-48959-8

**Table 1** (continued)

Nanoparticle source	Particle size	Dose	Exposure time	Cell line/in vivo models	Mechanism of toxicity	References (DOI)
Sigma-Aldrich	< 50 nm	0, 1, 5, 10 and 20 µg/ml	24 h	Human alveolar epithelial cell line (A549) Human cervix carcinoma cell line (HeLa S3)	Cytotoxicity and genotoxicity	10.1186/1743-8977-11-10
Sigma-Aldrich	< 50 nm	30 µg/ml	24 h	Human alveolar epithelial cell line (A549)	Autophagic cell death	10.1371/journal.pone.0043442
Sigma-Aldrich	50 nm	25 µg/ml	24 h	Human alveolar epithelial cell line (A549)	ROS production; Cytotoxicity	10.1021/nm202966t
Self-synthesized			36 h	Human alveolar epithelial cell line (A549)	Inflammation and apoptosis	10.1007/s10529-017-2463-6
Sigma-Aldrich	< 50 nm	0, 2, 4, 6, 8 and 10 µg/ml	24 h	Human colorectal adenocarcinoma cell line (HT29)	Cytotoxicity	10.1007/s00204-017-1976-z
Self-synthesized	30 ± 3.5 nm	0, 4, 6 and 12 µg/ml	24 h	Human breast cancer cells (MCF7)	Apoptosis; Protective autophagy activation	10.1016/j.bbagen.2013.08.011
Sigma-Aldrich	< 50 nm	1, 2, 5, 10, 20, and 40 µg/ml	24 h	Human airway epithelial cells (HEP-2)	Oxidative damage; ROS generation; Apoptosis	10.1007/s12011-022-03107-8
Nanostructured & Amorphous Materials Inc	50 nm	2.5–5.0 mg/kg (intratracheal instillation)	0, 1, 3, 7 d	Female C57BL/6 mice	Protein chlorination and acute lung inflammation	10.3390/ijms22179477
Sigma-Aldrich	< 50 nm	0, 25, 50, and 100 µg/kg (intratracheal instillation)	48 h	Female BALB/c mice Human airway epithelial cell line (NCI-H292)	Inflammatory responses and collagen deposition in lung tissue	10.1080/17435390.2018.1432778
Sigma-Aldrich	46.5 nm	1, 2.5, 5, and 10 mg/kg body weight (nasal instillation)	7, 14 and 28 d	C57BL/6 mice Alveolar and bronchial epithelial cell lines (A549 and BEAS-2B)	Pulmonary inflammation and fibrosis in mice Cytotoxicity and apoptosis in epithelial cells	10.1038/s41598-018-22556-7
Self-synthesized	40 nm to 110 nm	0, 0.625, 1.25, 2.5 and 5 µg/ml	48 h	Bladder cancer cell lines (T24, J82, 5637, and UMUC3)	ROS production; Cell cycle; Apoptosis	10.1038/cddis.2013.314
Intrinsic Materials Ltd	28.2 ± 13.7 nm	10 µg/ml	0, 1, 3, 6, 12, 24, 48 h	Alveolar epithelial cell line (A549)	Oxidative stress; Apoptosis	10.1186/s12989-016-0160-6
Self-synthesized	4, 24 nm	0, 0.5; 1.0; 1.5 and 2.0 mM	0, 1, 4, 24, 48 h	Alveolar epithelial cell line (A549)	ROS production; Cytotoxicity	10.1039/c5en00271k
Sigma-Aldrich	20–40 nm	0, 1, 5 and 10 µg/ml	4 h	Alveolar and bronchial epithelial cell lines (A549 and BEAS-2B)	DNA damage; Cytotoxicity	10.1002/smll.201201069

(SQSTM1/p62) [44]. After mitochondria dysfunction, excessive mtROS reduces mitochondrial membrane potential and induces PINK1 stabilization on the outer mitochondrial membrane (OMM) of damaged mitochondria, where it phosphorylates the ubiquitin of OMM proteins and then recruits mitophagy receptors to trigger mitophagy [44]. Defective mitophagy leads to accumulation of unwanted or damaged mitochondria, which results in excessive mtROS production and cell death via mitochondrial-dependent apoptosis pathway. Thus, clearance of damaged mitochondria via mitophagy is a potential therapeutic intervention to multiple diseases such as cancers, Alzheimer's disease and sepsis-induced heart failure [68–70]. Therefore, we hypothesized that the interplay between CuONPs-triggered mitochondrial fission and mitophagy might be involved in CuONPs-induced cytotoxicity. We showed that CuONPs exposure resulted in autophagosome recruitment to damaged mitochondria in vascular endothelial cells (Fig. 2A). Meanwhile, CuONPs upregulated PINK1 level in CuONPs-treated EA.hy926 cells (Fig. 3A). In addition, we found that PINK1 was recruited to damaged mitochondria (Fig. 3B) and *PINK1* knockdown inhibited clearance of damaged mitochondria and mtROS, consequently aggravated cell death in CuONPs-treated EA.hy926 cells (Fig. 3D–F). These data indicate that PINK1-dependent mitophagy facilitates removal of damaged mitochondria to appropriately mitigate oxidative stress and cell death in CuONPs-treated EA.hy926 cells. Recently, we reported that CuONPs exposure increased intracellular copper ions concentration both in vitro and in vivo model [16, 37]. Copper is an essential metal regulator of autophagy initial kinases ULK1/2, which directly interacts with ULK1/2 and enhances these kinases activity, consequently promotes autophagic flux [71]. Moreover, copper ions also upregulate PINK1 in primary chicken hepatocytes [72]. These findings indicate copper ions promotes PINK1-dependent autophagy/mitophagy in CuONPs-treated cells. However, the interactions among copper ions, mitochondrial fission and mitophagy need further investigations.

Subsequently, we identified that TAX1BP1 was the primary adaptor linking autophagosomes and ubiquitinated mitochondria via siRNA screening. Compared to other mitophagy receptor genes, *TAX1BP1* knockdown significantly aggravated CuONPs-induced cell death in EA.hy926 (Fig. 4A). Furthermore, TAX1BP1 was recruited to autophagosomes and mediated the connecting between damaged mitochondria and autophagosomes in CuONPs-treated EA.hy926 cells (Fig. 4B). *TAX1BP1* knockdown obviously caused more accumulation of damaged mitochondria and mtROS in

CuONPs-treated EA.hy926 cells (Fig. 4C, D). Shireen A. Sarraf et al. showed that TAX1BP1 participated in clearance of stress-induced protein aggregates [73]. TAX1BP1 also promotes autophagy and contributes to metabolic transition of activated immune T Cells [73]. These data indicate TAX1BP1 serves multiple functions in different cells or diseases model. Notably, NDP52 and OPTN, besides TAX1BP1, are the major receptors mediating PINK1-mediated mitophagy in human cervical cancer cell line (HeLa) [44]. In the current study, we showed that either *NDP52* or *OPTN* knockdown aggravated CuONPs-induced cell death, but their protective effects is less than *TAX1BP1* (Fig. 4A), suggesting the unique characteristics of mitophagy profile in CuONPs-treated vascular endothelial cells.

Considering mitophagy is a primary process facilitating clearance of damaged mitochondria and excessive mtROS induced by CuONPs, the means for the restoration of appropriate mitophagy is a promising strategy to protect against NPs exposure-induced toxicity. Urolithin A (UA) is a natural gut microbiome-derived metabolite. UA was reported to protect against oxidized low-density lipoprotein (ox-LDL)-induced vascular endothelial dysfunction by upregulating levels of nitric oxide and endothelial nitric oxide synthase, meanwhile markedly reducing the expression of inflammatory cytokines ICAM-1 and MCP-1 [74]. Several exciting studies have showed that UA is a first-in-class natural compound that inducing autophagy/mitophagy. It prolonged lifespan in *Caenorhabditis elegans* and improved muscle functions in mouse model by restoring mitochondrial respiratory capacity and removal of dysfunctional mitochondria [47, 50, 75]. Lee et al. also reported that UA inhibited mitochondrial calcium influx and mtROS accumulation in neuronal cells induced by high glucose, and consequently prevented diabetes mellitus-associated neurodegenerative disease pathogenesis [49]. Wang et al. showed that UA-induced mitophagy modulated mitochondrial unfolded protein response to attenuate sepsis-triggered myocardial stress [76]. These findings indicate UA is a promising therapy candidate for preventing NPs exposure-induced toxicity by maintaining mitochondrial and mtROS homeostasis. In this study, we demonstrated that UA promoted removal of damaged mitochondria and accelerated elimination of excessive mtROS in CuONPs-treated cells via PINK1-dependent pathway (Fig. 5). Furthermore, we revealed that UA significantly reduced damaged mitochondria mass and alleviated vascular injury in CuONPs-treated mice (Fig. 6D). These findings suggest mitophagy effectively alleviates CuONPs vascular toxicity. In addition, previous studies demonstrated

that UA regulated mitochondrial functions by maintaining mitochondrial calcium homeostasis, regulating cellular NAD<sup>+</sup> metabolism and activating mitochondrial unfolded protein response [49, 76, 77]. Thus, a combination of restoring mitochondrial functions and triggering mitophagy-mediated removal of damaged mitochondria is a promising strategy to alleviate NPs pulmonary exposure-induced vascular injury and related cardiovascular diseases.

## Material and Methods

### Materials and reagent

CuONPs (#544868), mitochondrial division inhibitor 1 (Mdivi-1, #M0199) and chloroquine (CQ, # C6628) were purchased from Sigma Aldrich (St. Louis, MO, USA). Wortmannin (Wort, #S2758) was purchased from Selleck Chemicals (Shanghai, China). Urolithin A (UA, #HY-100599) were purchased from Med-ChemExpress (Shanghai, China). MitoTracker™ Green FM(#M7514), MitoSOX™ Red (#M36008) and Dulbecco's modified Eagle's medium (DMEM, #11965-092) were purchased from Thermo Fisher Scientific (Waltham, MA, USA). Fetal bovine serum (FBS, #04-001-1ACS) was purchased from Biological Industries (Kibbutz Beit Haemek, Israel).

### Cell culture and treatment

The EA.hy926 cell line (established by fusing primary human umbilical vein cells with a thioguanine-resistant human lung carcinoma cell line A549) and HEK293T/17 lentiviral packaging cell line were purchased from the National Collection of Authenticated Cell Cultures (Shanghai, China). All cells were cultured in DMEM medium supplemented with 10% FBS and 100 U penicillin–streptomycin at 37 °C with 5% CO<sub>2</sub>. For CuONPs treatment, EA.hy926 cells were seeded in 12-well plates for overnight and then treated with different concentration of CuONPs for indicated time points. CuONPs was diluted in culture medium and vortexed for several seconds before treatment. For treatment with chemical materials, cells were pretreated with selected chemicals 1 h before CuONPs treatment.

### Generation of stable cell lines

The plasmids mCherry-Parkin (Plasmid #23956), GFP-LC3 (Plasmid #11546), psPAX2 (Plasmid #12260) and pMD2.G (Plasmid #12259) were obtained from Addgene (Cambridge, MA, USA). The plasmid pDsRed2-Mito was purchased from Clontech (Mountain View, CA, USA). The cDNA cloning and expression plasmid pCDH-CMV-MCSEF1-Puro was obtained

from System Biosciences (Palo Alto, CA, USA). For lentiviral vectors construction, gene fragments were PCR amplified using I-5™ Hi-Fi DNA Polymerase (#PDP-100, MCLAB, San Francisco, CA, USA) and then inserted into pCDH-CMV-MCSEF1-Puro lentivirus vector using pEASY®-Basic Seamless Cloning and Assembly Kit (#CU201-02, TransGen Biotech, Beijing, China). Then, the sequenced lentivirus plasmid was co-transfected with packaging plasmids psPAX2 and pMD2.G into HEK293T/17 using NEOFECT™ DNA transfection reagent (Neofect biotech, Beijing, China) for 48–72 h. The culture supernatants were harvested and inoculated into EA.hy926 cells. The stable cell lines were generated by two rounds of puromycin selection.

### Animals and treatment

The physical–chemical characteristics of CuONPs were described in our previous study [37]. For preparation of CuONPs suspension, CuONPs were firstly diluted in serum solution (composed of 2% heat-inactivated sibling mouse serum in MilliQ water) to the concentration of 2 mg/mL. Then CuONPs solution was sonicated for 20 min with an ultrasonic cleaner. CuONPs suspension was freshly prepared before intratracheal instillation to avoid dissolution of CuONPs to copper ions. Before instillation, CuONPs suspension was thoroughly vortexed for 30 s to avoid any agglomeration.

This study was approved by the Institutional Animal Care and Use Committee of Chongqing Medical University. Specific-pathogen-free C57BL/6 J male mice (aged 8–12 weeks, weight 18–22 g) were purchased from the Experimental Animal Center of Chongqing Medical University. All animals were randomized into the following 4 groups: Control, CuONPs (5 mg/kg), UA (30 mg/kg), and CuONPs (5 mg/kg) + UA (30 mg/kg). The animals were housed in groups in controlled environmental temperature. After 1-week of habituation, the mice in UA group and CuONPs + UA group were treated daily orally with UA (30 mg/kg) by gavage for 7 days. On the eighth day, the mice in CuONPs group and CuONPs + UA group were intratracheally instilled CuONPs after anesthetization with 1% pentobarbital sodium, meanwhile the mice in UA group and CuONPs + UA group were continuously treated with UA (30 mg/kg) by gavage for 3 days. Finally, the C57BL/6 J mice were sacrificed and the abdominal aorta were obtained.

### Transmission electron microscopy (TEM) imaging

After CuONPs treatment, cells were centrifuged at 106 × g for 5 min after trypsinization and then fixed with

4% glutaraldehyde for 2 h at 4 °C. Next, cells were post-fixed with 1% osmium tetroxide for 1 h at 4 °C. Subsequently, cells were dehydrated in a grade series of alcohol and acetone followed by embedment in Epon 816 (Electron Microscopy Sciences, Hatfield, PA, USA). Ultrathin sections were obtained by using a Leica EM UC7 Ultramicrotome (Leica Microsystems, Buffalo Grove, IL, USA) and stained with uranyl acetate and lead citrate. TEM images were taken with a JEM-1400 Plus transmission electron microscope (JEOL Ltd. Tokyo, Japan).

### Western blotting

The cells seeded in 12-well plate were washed with cold phosphate-buffered saline (PBS) buffer and lysed with 2 × protein lysis buffer (2% SDS, 5% 2-mercaptoethanol, 0.5% sucrose and 0.2% bromophenol blue). Mouse vascular tissues were washed with cold PBS and lysed with RIPA buffer containing protease inhibitors (Beyotime, Shanghai, China, #P0013B). Then, lysed tissues were homogenized with dounce homogenizer and centrifuged at 10,000 × g for 10 min at 4 °C. Protein lysates were boiled for 5 min and separated in 8%-12% polyacrylamide gels. After electrophoresis, proteins were transferred from gel to polyvinylidene fluoride membrane (Merck Millipore, Billerica, MA, USA). The membrane was incubated with 5% non-fat milk, incubated separately with primary antibodies diluted in blocking buffer for overnight at 4 °C and then probed with secondary antibody diluted in TBST (Tris Buffered Saline with Tween 20) at room temperature for 1 h. After washing with TBST, the membranes were incubated with BeyoECL Star substrates (Beyotime, #P0018AM). All antibodies used in this study were listed as below: LC3B (1:3,000, Sigma Aldrich, #L7543), ATP5B (1:500, Santa Cruz Biotechnology, #sc-166462), TOM20 (1:1,000, Proteintech, Wuhan, China, #11802-1-AP), TIM23 (1:1,000, Santa Cruz Biotechnology, #sc-514463), VDAC1(1:2,000, Bimake, #A5224), FIS1 (1:3,000, Proteintech, #10956-1-AP), DRP1 (1:4,000, Proteintech, #12957-1-AP), p-DRP1 (1:1,000, Cell Signaling Technology, #3455S), GAPDH (1:10,000, Proteintech, #60004-1-Ig), Actin (1:10,000, TransGen Biotech, Beijing, China, #HC201-01), HRP-conjugated goat anti-mouse IgG (1:10,000, TransGen Biotech, #HS201-01) and HRP-conjugated goat antirabbit IgG (1:10,000, TransGen Biotech, #HS101-01).

### Flow cytometry

After treatment, cells seeded in 12-well plate were washed with PBS and incubated with 0.25% trypsin/EDTA solution (Beyotime, #C0201). Then, cells were pipetted and collected through centrifugation, and incubated with MitoTracker™ Green FM (500 nM, Thermo fisher, #M7514) or MitoSOX™ Red (5 μM, Thermo fisher,

#M36008) for 15–30 min at 37 °C in a cell culture incubator. The stained cells were re-pelleted and then detected under a CytoFLEX flow cytometry (Beckman Coulter, Miami, FL, USA). The cytometry data were analyzed by FlowJo™ v10 Software BD Biosciences (San Jose, CA, USA).

### Immunofluorescence cell staining

The cells were seeded on a sterilized coverslip in a 24-well plate for overnight. After treatment, cells were fixed in 4% paraformaldehyde for 15 min at room temperature, permeabilized with 0.2% Triton X-100 for 10 min at room temperature, and then blocked with blocking buffer (2% BSA and 0.3 M glycine in PBS) for 1 h at room temperature. The cells were then incubated with primary antibodies diluted in blocking buffer for overnight at 4 °C. After washing three times with PBS, cells were incubated with Alexa Fluor-conjugated secondary antibodies and 4',6-diamidino-2-phenylindole (DAPI, Molecular Probes, Eugene, OR, USA) diluted in blocking buffer for 1 h at room temperature. After washing with PBS, cells were sealed with nail polish. Fluorescence images were taken under a Nikon A1R+/A1 Confocal Microscope (Nikon, Tokyo, Japan). The antibodies used in this study are as follows: ATP5B (1:25, Santa Cruz Biotechnology, #sc-166462), TAX1BP1(1:50, Proteintech, #14424-1-AP), Alexa Fluor 594-conjugated donkey anti-rabbit IgG (1:500, Molecular Probes, #A-21207) and Alexa Fluor 647-conjugated donkey anti-rabbit IgG (1:500, Molecular Probes, #A-21245).

### Cell viability assays

The cells were cultured in 96-well plates at a density of  $1 \times 10^4$ /well for overnight. After treatment for indicated time points and concentrations described in figure captions, CellTiter 96® Aqueous One Solution Reagent (#G3581, Promega, Madison, WI, USA) was diluted in culture media and added to each well of culture plates. The plate was incubated at 37 °C for 1 h and the absorbance of each well was measured in a VERS Amax

**Table 2** The list of siRNA sequences used in this study

Target	Sequence
PINK1 (human)	GAGAAGUGUUGUGUGGAAATT
p62/SQSTM1 (human)	GCAUUGAAGUUGAUUCGATT
NDP52 (human)	GCUUGUUCAGGAGAUCAATT
NBR1 (human)	GCUCAAGAUGAAGUUCGATT
TAX1BP1 (human)	CAAAGAAUUGCUGACAAATT
Optineurin (human)	GGAAGUUUACUGUUCGUAUTT
GFP (human)	GCAGCACGACUUCUUCAGTT

**Table 3** The list of qPCR primers used in this study

Gene names	Forward primer(5'-3')	Reverse primer(5'-3')
<i>NDP52</i>	CTGCTATGTGGATGAGGAT	ATGTCTGAGTTCTGCTTCT
<i>NBR1</i>	ACAGCATAAGTGACATCCT	TTCTGGTATGGTAACTGGTAA
<i>TAX1BP1</i>	GCCAAGAGTTACCTTCCTA	TTGACTGTTGATCCTTCCA
<i>OPTN</i>	GCTCCTCAGAAGATTCCCT	TGCTCTATATTTAGACAATGC
<i>p62</i>	TCGGATAACTGTTCCAGGAG	CGGATTCTGGCATCTGTA
<i>PINK1</i>	GCCATCTTGAACACAATGA	CTGTAAGTGAAGTCTCCA
<i>TBP</i>	ATCAGTGCCGTGGTTCGT	TTCGGAGAGTTCTGGGATTG

Microplate Reader (Molecular Devices, Sunnyvale, CA, USA) set at 490 nm and 630 nm. All assays were conducted in triplicate and repeated three times.

### Transfecting siRNA using lipofectamine™ RNAiMAX

Before siRNA duplex transfection, cells seeded in 12-well plates for overnight were added fresh culture media. The siRNA duplex and Lipofectamine RNAiMAX transfection reagent (Invitrogen, Waltham, MA, USA) were diluted in Opti-MEM media (GIBCO, Grand Island, NY, USA), respectively. Then, the diluted siRNA duplex and Lipofectamine RNAiMAX were mixed gently and incubated for 10–20 min at room temperature. Finally, the RNAi duplex-Lipofectamine™ RNAiMAX complexes were added into plate well. After siRNA transfection for 36–48 h, RNAi efficiency was analyzed by real-time quantitative PCR or western blotting. All siRNA duplex used in this study were synthesized by GenePharma (Shanghai, China) and the target sequences were listed in Table 2.

### Real-time quantitative PCR (qPCR)

Total RNA was extracted from cells using Eastep Super Total RNA Extraction Kit (# RC112-01, Vazyme, Nanjing, China) and then the purified RNA was reversely transcribed to cDNA with HiScript II Q RT SuperMix for qPCR (+gDNA wiper) (#R223-01, Vazyme) according to the manufacturer protocols. qPCR amplification assays were performed with ChamQ Universal SYBR qPCR Master Mix (#Q711-03, Vazyme) under a CFX Connect Real-Time PCR Detection System (Bio-Rad, CA, USA). The *TBP* (TATA-Box Binding Protein) was chosen as housekeeping reference gene. The specific primers were synthesized by Sangon (Shanghai, China) and shown in Table 3.

### Statistical analysis

The data were shown as mean ± standard deviation (S.D.). Each experiment was repeated three times.

Data were analyzed by two-tailed unpaired Student's *t*-test for two groups comparisons or one-way ANOVA followed by Tukey's test for comparisons of parameters among multiple groups. All statistical analyses were taken with GraphPad Prism 5.0 software (San Diego, CA, USA). \**p* < 0.05 was considered statistical significance.

### Acknowledgements

We thank Xiaoyun Dou for her help in confocal microscopy and appreciate all Dongsheng lab members for their help in experiments.

### Authors' contributions

JZ and ZZ conceived and designed this project. YF, ZC, NL, MZ, PW, LZ, XD and SH contributed to major experiments. LM and GX helped in electron microscopy and confocal microscope. XQ, XJ and CC helped to data analysis. JZ and ZZ wrote manuscript with input from all authors. All authors have read and approved the final manuscript.

### Funding

This work was supported partly by the National Natural Science Foundation of China (81500343 and 81903358), the Chongqing Talents: Exceptional Young Talents Project (CQYC2020058650), the Natural Science Foundation of Chongqing (cstc2018jcyjAX0355, cstc2020jcyj-msxmX0155 and cstc2021ycjh-bgzxm0105), the Science and Technology Research Program of Chongqing Municipal Education Commission (KJQN201900421, KJQN202000423, KJCXZD2020020 and KJQN202100405) and Graduate top-notch program of Chongqing Medical University (BJRC202130). Jun Zhang, Zhen Zou and Chengzhi Chen are supported by Chongqing Bayu Talented Young Scholar program.

### Availability of data and materials

The authors declare that data related to this study are provided upon request.

### Declarations

#### Ethical approval and consent to participate

This study has been officially approved by Chongqing Medical University and the protocol was performed in accordance with the recommendations of the Guide for the Care and Use of Laboratory Animals of the Chongqing Medical University. The proof/certificate of approval for animal experiments is available upon request.

#### Consent for publication

Not Applicable.

#### Competing interests

The authors declare that they have no competing financial interests.

#### Author details

<sup>1</sup>Molecular Biology Laboratory of Respiratory Disease, Institute of Life Sciences, Chongqing Medical University, Chongqing 400016, People's Republic of China. <sup>2</sup>Department of Cardiovascular Medicine, Children's Hospital of Chongqing Medical University, Chongqing 400014, People's Republic of China. <sup>3</sup>Chongqing Key Laboratory of Pediatrics, Children's Hospital of Chongqing Medical University, Chongqing 400014, People's Republic of China. <sup>4</sup>College of Pharmacy, Chongqing Medical University, Chongqing 400016, China. <sup>5</sup>Department of Pharmacy, The First Affiliated Hospital of Chongqing Medical University, Chongqing 400016, China. <sup>6</sup>Center of Experimental Teaching for Public Health, Experimental Teaching and Management Center, Chongqing Medical University, Chongqing 400016, People's Republic of China. <sup>7</sup>Department of Occupational and Environmental Health, School of Public Health and Management, Chongqing Medical University, Chongqing 400016, China. <sup>8</sup>Dongsheng Lung-Brain Diseases Joint Laboratory, Chongqing Medical University, Chongqing 400016, China.

Received: 20 January 2022 Accepted: 26 February 2022  
Published online: 19 March 2022

## References

- Gawande MB, Goswami A, Felpin FX, Asefa T, Huang X, Silva R, et al. Cu and Cu-based nanoparticles: synthesis and applications in catalysis. *Chem Rev.* 2016;116(6):3722–811. <https://doi.org/10.1021/acs.chemrev.5b00482>.
- Verma N, Kumar N. Synthesis and biomedical applications of copper oxide nanoparticles: an expanding horizon. *ACS Biomater Sci Eng.* 2019;5(3):1170–88. <https://doi.org/10.1021/acsbiomaterials.8b01092>.
- Xu H, Yuan R, Liu X, Li X, Qiao G, Li C, et al. Zn-doped CuO nanocomposites inhibit tumor growth by NF-kappaB pathway cross-linked autophagy and apoptosis. *Nanomedicine (Lond).* 2019;14(2):131–49. <https://doi.org/10.2217/nmm-2018-0366>.
- Mani VM, Kalaivani S, Sabarathinam S, Vasuki M, Soundari A, Ayyappa Das MP, et al. Copper oxide nanoparticles synthesized from an endophytic fungus *Aspergillus terreus*: bioactivity and anti-cancer evaluations. *Environ Res.* 2021;201:111502. <https://doi.org/10.1016/j.envres.2021.111502>.
- Chen H, Feng X, Gao L, Mickymaray S, Paramasivam A, Abdulaziz Alfaiz F, et al. Inhibiting the PI3K/AKT/mTOR signalling pathway with copper oxide nanoparticles from *Houttuynia cordata* plant: attenuating the proliferation of cervical cancer cells. *Artif Cells Nanomed Biotechnol.* 2021;49(1):240–9. <https://doi.org/10.1080/21691401.2021.1890101>.
- Ren G, Hu D, Cheng EW, Vargas-Reus MA, Reip P, Allaker RP. Characterisation of copper oxide nanoparticles for antimicrobial applications. *Int J Antimicrob Agents.* 2009;33(6):587–90. <https://doi.org/10.1016/j.ijant.2008.12.004>.
- Imani SM, Ladouceur L, Marshall T, MacLachlan R, Soleymani L, Didar TF. Antimicrobial nanomaterials and coatings: current mechanisms and future perspectives to control the spread of viruses including SARS-CoV-2. *ACS Nano.* 2020;14(10):12341–69. <https://doi.org/10.1021/acsnano.0c05937>.
- Tortella GR, Pieretti JC, Rubilar O, Fernandez-Baldo M, Benavides-Mendoza A, Diez MC, et al. Silver, copper and copper oxide nanoparticles in the fight against human viruses: progress and perspectives. *Crit Rev Biotechnol.* 2021. <https://doi.org/10.1080/07388551.2021.1939260>.
- Merkel P, Long S, McInerney GM, Sotiriou GA. Antiviral activity of silver, copper oxide and zinc oxide nanoparticle coatings against SARS-CoV-2. *Nanomaterials (Basel).* 2021. <https://doi.org/10.3390/nano11051312>.
- Qiao Y, He J, Chen W, Yu Y, Li W, Du Z, et al. Light-activatable synergistic therapy of drug-resistant bacteria-infected cutaneous chronic wounds and nonhealing keratitis by cupriferous hollow nanoshells. *ACS Nano.* 2020;14(3):3299–315. <https://doi.org/10.1021/acsnano.9b08930>.
- Sen S, Sarkar K. Effective biocidal and wound healing cogency of biocompatible glutathione: citrate-capped copper oxide nanoparticles against multidrug-resistant pathogenic enterobacteria. *Microb Drug Resist.* 2021;27(5):616–27. <https://doi.org/10.1089/mdr.2020.0131>.
- Sun T, Yan Y, Zhao Y, Guo F, Jiang C. Copper oxide nanoparticles induce autophagic cell death in A549 cells. *PLoS ONE.* 2012;7(8):e43442. <https://doi.org/10.1371/journal.pone.0043442>.
- Lowry GV, Gregory KB, Apte SC, Lead JR. Transformations of nanomaterials in the environment. *Environ Sci Technol.* 2012;46(13):6893–9. <https://doi.org/10.1021/es300839e>.
- Setyawati MI, Zhao Z, Ng KW. Transformation of nanomaterials and its implications in gut nanotoxicology. *Small.* 2020;16(36):e2001246. <https://doi.org/10.1002/sml.202001246>.
- Wang Z, von dem Bussche A, Kabadi PK, Kane AB, Hurt RH. Biological and environmental transformations of copper-based nanomaterials. *ACS Nano.* 2013;7(10):8715–27. <https://doi.org/10.1021/nn403080y>.
- Zhang J, Zou Z, Wang B, Xu G, Wu Q, Zhang Y, et al. Lysosomal deposition of copper oxide nanoparticles triggers HUVEC cells death. *Biomaterials.* 2018;161:228–39. <https://doi.org/10.1016/j.biomaterials.2018.01.048>.
- Hadrup N, Zheronkov V, Jacobsen NR, Voss C, Strunz M, Ansari M, et al. Acute Phase response as a biological mechanism-of-action of (nano) particle-induced cardiovascular disease. *Small.* 2020;16(21):e1907476. <https://doi.org/10.1002/sml.201907476>.
- Liu X, Wei W, Liu Z, Song E, Lou J, Feng L, et al. Serum apolipoprotein A-I depletion is causative to silica nanoparticles-induced cardiovascular damage. *Proc Natl Acad Sci U S A.* 2021. <https://doi.org/10.1073/pnas.2108131118>.
- Raftis JB, Miller MR. Nanoparticle translocation and multi-organ toxicity: a particularly small problem. *Nano Today.* 2019;26:8–12. <https://doi.org/10.1016/j.nantod.2019.03.010>.
- Mills NL, Miller MR, Lucking AJ, Beveridge J, Flint L, Boere AJ, et al. Combustion-derived nanoparticulate induces the adverse vascular effects of diesel exhaust inhalation. *Eur Heart J.* 2011;32(21):2660–71. <https://doi.org/10.1093/eurheartj/ehr195>.
- Kang GS, Gillespie PA, Gunnison A, Moreira AL, Tchou-Wong KM, Chen LC. Long-term inhalation exposure to nickel nanoparticles exacerbated atherosclerosis in a susceptible mouse model. *Environ Health Perspect.* 2011;119(2):176–81. <https://doi.org/10.1289/ehp.1002508>.
- Lee DK, Jang HS, Chung H, Jeon S, Jeong J, Choi JH, et al. Aggravation of atherosclerosis by pulmonary exposure to indium oxide nanoparticles. *Nanotoxicology.* 2020;14(3):355–71. <https://doi.org/10.1080/17435390.2019.1704590>.
- Ma R, Qi Y, Zhao X, Li X, Sun X, Niu P, et al. Amorphous silica nanoparticles accelerated atherosclerotic lesion progression in ApoE(-/-) mice through endoplasmic reticulum stress-mediated CD36 up-regulation in macrophage. *Part Fibre Toxicol.* 2020;17(1):50. <https://doi.org/10.1186/s12989-020-00380-0>.
- Kruger-Genge A, Blocki A, Franke RP, Jung F. Vascular endothelial cell biology: an update. *Int J Mol Sci.* 2019. <https://doi.org/10.3390/ijms20184411>.
- Miller MR, Raftis JB, Langrish JP, McLean SG, Samutritai P, Connell SP, et al. Inhaled nanoparticles accumulate at sites of vascular disease. *ACS Nano.* 2017;11(5):4542–52. <https://doi.org/10.1021/acsnano.6b08551>.
- Chan DC. Mitochondrial dynamics and its involvement in disease. *Annu Rev Pathol.* 2020;15:235–59. <https://doi.org/10.1146/annurev-pathm.echdis-012419-032711>.
- Russell OM, Gorman GS, Lightowlers RN, Turnbull DM. Mitochondrial diseases: hope for the future. *Cell.* 2020;181(1):168–88. <https://doi.org/10.1016/j.cell.2020.02.051>.
- He H, Xiao S, Xu G, Wang B, Zou Z, Qin X, et al. The NADPH oxidase 4 protects vascular endothelial cells from copper oxide nanoparticles-induced oxidative stress and cell death. *Life Sci.* 2020;252:117571. <https://doi.org/10.1016/j.lfs.2020.117571>.
- Zhang J, Wang B, Wang H, He H, Wu Q, Qin X, et al. Disruption of the superoxide anions-mitophagy regulation axis mediates copper oxide nanoparticles-induced vascular endothelial cell death. *Free Radic Biol Med.* 2018;129:268–78. <https://doi.org/10.1016/j.freeradbiomed.2018.09.032>.
- Wang K, Klionsky DJ. Mitochondria removal by autophagy. *Autophagy.* 2011;7(3):297–300. <https://doi.org/10.4161/autof.7.3.14502>.
- Youle RJ, Narendra DP. Mechanisms of mitophagy. *Nat Rev Mol Cell Biol.* 2011;12(1):9–14. <https://doi.org/10.1038/nrm3028>.
- Qi Y, Ma R, Li X, Lv S, Liu X, Abulikemu A, et al. Disturbed mitochondrial quality control involved in hepatocytotoxicity induced by silica nanoparticles. *Nanoscale.* 2020;12(24):13034–45. <https://doi.org/10.1039/d0nr01893g>.
- Li J, Chang X, Shang M, Niu S, Zhang W, Li Y, et al. The crosstalk between DRP1-dependent mitochondrial fission and oxidative stress triggers hepatocyte apoptosis induced by silver nanoparticles. *Nanoscale.* 2021;13(28):12356–69. <https://doi.org/10.1039/d1nr02153b>.
- Wu D, Lu J, Ma Y, Cao Y, Zhang T. Mitochondrial dynamics and mitophagy involved in MPA-capped CdTe quantum dots-induced toxicity in the human liver carcinoma (HepG2) cell line. *Environ Pollut.* 2021;274:115681. <https://doi.org/10.1016/j.envpol.2020.115681>.
- Li J, Chang X, Shang M, Niu S, Zhang W, Zhang B, et al. Mitophagy-lysosomal pathway is involved in silver nanoparticle-induced apoptosis in A549 cells. *Ecotoxicol Environ Saf.* 2021;208:111463. <https://doi.org/10.1016/j.ecoenv.2020.111463>.
- Wei L, Wang J, Chen A, Liu J, Feng X, Shao L. Involvement of PINK1/parkin-mediated mitophagy in ZnO nanoparticle-induced toxicity in BV-2 cells. *Int J Nanomedicine.* 2017;12:1891–903. <https://doi.org/10.2147/IJN.S129375>.
- Xiao J, Tu B, Zhou X, Jiang X, Xu G, Zhang J, et al. Autophagy deficiency exacerbates acute lung injury induced by copper oxide nanoparticles.

- J Nanobiotechnology. 2021;19(1):162. <https://doi.org/10.1186/s12951-021-00909-1>.
38. Wai T, Langer T. Mitochondrial dynamics and metabolic regulation. *Trends Endocrinol Metab.* 2016;27(2):105–17. <https://doi.org/10.1016/j.tem.2015.12.001>.
  39. Palikaras K, Lionaki E, Tavernarakis N. Mechanisms of mitophagy in cellular homeostasis, physiology and pathology. *Nat Cell Biol.* 2018;20(9):1013–22. <https://doi.org/10.1038/s41556-018-0176-2>.
  40. Liu L, Li Y, Wang J, Zhang D, Wu H, Li W, et al. Mitophagy receptor FUNDC1 is regulated by PGC-1 $\alpha$ /NRF1 to fine tune mitochondrial homeostasis. *EMBO Rep.* 2021;22(3):e50629. <https://doi.org/10.15252/embr.202050629>.
  41. Takahashi D, Moriyama J, Nakamura T, Miki E, Takahashi E, Sato A, et al. AUTACs: cargo-specific degraders using selective autophagy. *Mol Cell.* 2019;76(5):797–810 e10. <https://doi.org/10.1016/j.molcel.2019.09.009>.
  42. Wang Y, Nartiss Y, Steipe B, McQuibban GA, Kim PK. ROS-induced mitochondrial depolarization initiates PARK2/PARKIN-dependent mitochondrial degradation by autophagy. *Autophagy.* 2012;8(10):1462–76. <https://doi.org/10.4161/auto.21211>.
  43. Geisler S, Holmstrom KM, Skujat D, Fiesel FC, Kahle PJ, et al. PINK1/Parkin-mediated mitophagy is dependent on VDAC1 and p62/SQSTM1. *Nat Cell Biol.* 2010;12(2):119–31. <https://doi.org/10.1038/ncb2012>.
  44. Lazarou M, Sliter DA, Kane LA, Sarraf SA, Wang C, Burman JL, et al. The ubiquitin kinase PINK1 recruits autophagy receptors to induce mitophagy. *Nature.* 2015;524(7565):309–14. <https://doi.org/10.1038/nature14893>.
  45. Richter B, Sliter DA, Herhaus L, Stolz A, Wang C, Beli P, et al. Phosphorylation of OPTN by TBK1 enhances its binding to Ub chains and promotes selective autophagy of damaged mitochondria. *Proc Natl Acad Sci U S A.* 2016;113(15):4039–44. <https://doi.org/10.1073/pnas.1523926113>.
  46. D'Amico D, Andreux PA, Valdes P, Singh A, Rinsch C, Auwerx J. Impact of the natural compound urolithin A on health, disease, and aging. *Trends Mol Med.* 2021;27(7):687–99. <https://doi.org/10.1016/j.molmed.2021.04.009>.
  47. Ryu D, Mouchiroud L, Andreux PA, Katsyuba E, Moullan N, Nicolet-Dit-Felix AA, et al. Urolithin A induces mitophagy and prolongs lifespan in *C. elegans* and increases muscle function in rodents. *Nat Med.* 2016;22(8):879–88. <https://doi.org/10.1038/nm.4132>.
  48. Fang EF, Hou Y, Palikaras K, Adriaanse BA, Kerr JS, Yang B, et al. Mitophagy inhibits amyloid-beta and tau pathology and reverses cognitive deficits in models of Alzheimer's disease. *Nat Neurosci.* 2019;22(3):401–12. <https://doi.org/10.1038/s41593-018-0332-9>.
  49. Lee HJ, Jung YH, Choi GE, Kim JS, Chae CW, Lim JR, et al. Urolithin A suppresses high glucose-induced neuronal amyloidogenesis by modulating TGM2-dependent ER-mitochondria contacts and calcium homeostasis. *Cell Death Differ.* 2021;28(1):184–202. <https://doi.org/10.1038/s41418-020-0593-1>.
  50. Luan P, D'Amico D, Andreux PA, Laurila PP, Wohlwend M, Li H, et al. Urolithin A improves muscle function by inducing mitophagy in muscular dystrophy. *Sci Transl Med.* 2021. <https://doi.org/10.1126/scitranslmed.abb0319>.
  51. Spinelli JB, Haigis MC. The multifaceted contributions of mitochondria to cellular metabolism. *Nat Cell Biol.* 2018;20(7):745–54. <https://doi.org/10.1038/s41556-018-0124-1>.
  52. Murphy MP, Hartley RC. Mitochondria as a therapeutic target for common pathologies. *Nat Rev Drug Discov.* 2018;17(12):865–86. <https://doi.org/10.1038/nrd.2018.174>.
  53. Jannesari M, Akhavan O, Madaah Hosseini HR, Bakhshi B. Graphene/CuO2 nanoshuttles with controllable release of oxygen nanobubbles promoting interruption of bacterial respiration. *ACS Appl Mater Interfaces.* 2020;12(32):35813–25. <https://doi.org/10.1021/acsami.0c05732>.
  54. Youle RJ, van der Bliek AM. Mitochondrial fission, fusion, and stress. *Science.* 2012;337(6098):1062–5. <https://doi.org/10.1126/science.1219855>.
  55. Sprenger HG, Langer T. The good and the bad of mitochondrial breakups. *Trends Cell Biol.* 2019;29(11):888–900. <https://doi.org/10.1016/j.tcb.2019.08.003>.
  56. Ma W, He S, Ma H, Jiang H, Yan N, Zhu L, et al. Silver nanoparticle exposure causes pulmonary structural damage and mitochondrial dynamic imbalance in the rat: protective effects of sodium selenite. *Int J Nanomedicine.* 2020;15:633–45. <https://doi.org/10.2147/IJN.S232986>.
  57. He H, Zou Z, Wang B, Xu G, Chen C, Qin X, et al. Copper oxide nanoparticles induce oxidative DNA damage and cell death via copper ion-mediated P38 MAPK activation in vascular endothelial cells. *Int J Nanomedicine.* 2020;15:3291–302. <https://doi.org/10.2147/IJN.S241157>.
  58. Makino A, Scott BT, Dillmann WH. Mitochondrial fragmentation and superoxide anion production in coronary endothelial cells from a mouse model of type 1 diabetes. *Diabetologia.* 2010;53(8):1783–94. <https://doi.org/10.1007/s00125-010-1770-4>.
  59. Giedt RJ, Yang C, Zweier JL, Matzavinos A, Alevriadou BR. Mitochondrial fission in endothelial cells after simulated ischemia/reperfusion: role of nitric oxide and reactive oxygen species. *Free Radic Biol Med.* 2012;52(2):348–56. <https://doi.org/10.1016/j.freeradbiomed.2011.10.491>.
  60. Yu T, Sheu SS, Robotham JL, Yoon Y. Mitochondrial fission mediates high glucose-induced cell death through elevated production of reactive oxygen species. *Cardiovasc Res.* 2008;79(2):341–51. <https://doi.org/10.1093/cvr/cvn104>.
  61. Sheridan C, Delivani P, Cullen SP, Martin SJ. Bax- or Bak-induced mitochondrial fission can be uncoupled from cytochrome C release. *Mol Cell.* 2008;31(4):570–85. <https://doi.org/10.1016/j.molcel.2008.08.002>.
  62. Moyzis AG, Lally NS, Liang W, Leon LJ, Najor RH, Orogo AM, et al. McI-1-mediated mitochondrial fission protects against stress but impairs cardiac adaptation to exercise. *J Mol Cell Cardiol.* 2020;146:109–20. <https://doi.org/10.1016/j.yjmcc.2020.07.009>.
  63. Morita M, Prudent J, Basu K, Goyon V, Katsumura S, Hulea L, et al. mTOR Controls Mitochondrial Dynamics and Cell Survival via MTFP1. *Mol Cell.* 2017;67(6):922–35 e5. <https://doi.org/10.1016/j.molcel.2017.08.013>.
  64. Mao K, Klionsky DJ. Mitochondrial fission facilitates mitophagy in *Saccharomyces cerevisiae*. *Autophagy.* 2013;9(11):1900–1. <https://doi.org/10.4161/auto.25804>.
  65. Li E, Li X, Huang J, Xu C, Liang Q, Ren K, et al. BMAL1 regulates mitochondrial fission and mitophagy through mitochondrial protein BNIP3 and is critical in the development of dilated cardiomyopathy. *Protein Cell.* 2020;11(9):661–79. <https://doi.org/10.1007/s13238-020-00713-x>.
  66. da Silva Rosa SC, Martens MD, Field JT, Nguyen L, Kereliuk SM, Hai Y, et al. BNIP3L/Nix-induced mitochondrial fission, mitophagy, and impaired myocyte glucose uptake are abrogated by PRKA/PKA phosphorylation. *Autophagy.* 2021;17(9):2257–72. <https://doi.org/10.1080/15548627.2020.1821548>.
  67. Wang J, Gao S, Wang S, Xu Z, Wei L. Zinc oxide nanoparticles induce toxicity in CAL 27 oral cancer cell lines by activating PINK1/Parkin-mediated mitophagy. *Int J Nanomedicine.* 2018;13:3441–50. <https://doi.org/10.2147/IJN.S165699>.
  68. Sun Y, Yao X, Zhang QJ, Zhu M, Liu ZP, Ci B, et al. Beclin-1-dependent autophagy protects the heart during sepsis. *Circulation.* 2018;138(20):2247–62. <https://doi.org/10.1161/CIRCULATIONAHA.117.032821>.
  69. Cen X, Chen Y, Xu X, Wu R, He F, Zhao Q, et al. Pharmacological targeting of MCL-1 promotes mitophagy and improves disease pathologies in an Alzheimer's disease mouse model. *Nat Commun.* 2020;11(1):5731. <https://doi.org/10.1038/s41467-020-19547-6>.
  70. Boyle KA, Van Wickle J, Hill RB, Marchese A, Kalyanaraman B, Dwinell MB. Mitochondria-targeted drugs stimulate mitophagy and abrogate colon cancer cell proliferation. *J Biol Chem.* 2018;293(38):14891–904. <https://doi.org/10.1074/jbc.RA117.001469>.
  71. Tsang T, Posimo JM, Gudiel AA, Cicchini M, Feldser DM, Brady DC. Copper is an essential regulator of the autophagic kinases ULK1/2 to drive lung adenocarcinoma. *Nat Cell Biol.* 2020;22(4):412–24. <https://doi.org/10.1038/s41556-020-0481-4>.
  72. Yang F, Liao J, Yu W, Qiao N, Guo J, Han Q, et al. Exposure to copper induces mitochondria-mediated apoptosis by inhibiting mitophagy and the PINK1/parkin pathway in chicken (*Gallus gallus*) livers. *J Hazard Mater.* 2021;408:124888. <https://doi.org/10.1016/j.jhazmat.2020.124888>.
  73. Whang MI, Tavares RM, Benjamin DI, Kattah MG, Advincula R, Nomura DK, et al. The ubiquitin binding protein TAX1BP1 mediates autophagosome induction and the metabolic transition of activated T cells. *Immunity.* 2017;46(3):405–20. <https://doi.org/10.1016/j.immuni.2017.02.018>.
  74. Han QA, Yan C, Wang L, Li G, Xu Y, Xia X. Urolithin A attenuates ox-LDL-induced endothelial dysfunction partly by modulating microRNA-27 and ERK/PPAR-gamma pathway. *Mol Nutr Food Res.* 2016;60(9):1933–43. <https://doi.org/10.1002/mnfr.201500827>.
  75. Raj SD, Fann DY, Wong E, Kennedy BK. Natural products as geroprotectors: an autophagy perspective. *Med Res Rev.* 2021;41(6):3118–55. <https://doi.org/10.1002/med.21815>.
  76. Wang Y, Jasper H, Toan S, Muid D, Chang X, Zhou H. Mitophagy coordinates the mitochondrial unfolded protein response to attenuate

inflammation-mediated myocardial injury. *Redox Biol.* 2021;45: 102049. <https://doi.org/10.1016/j.redox.2021.102049>.

77. Ghosh N, Das A, Biswas N, Gnyawali S, Singh K, Gorain M, et al. Urolithin A augments angiogenic pathways in skeletal muscle by bolstering NAD(+) and SIRT1. *Sci Rep.* 2020;10(1):20184. <https://doi.org/10.1038/s41598-020-76564-7>.

### **Publisher's Note**

Springer Nature remains neutral with regard to jurisdictional claims in published maps and institutional affiliations.

**Ready to submit your research? Choose BMC and benefit from:**

- fast, convenient online submission
- thorough peer review by experienced researchers in your field
- rapid publication on acceptance
- support for research data, including large and complex data types
- gold Open Access which fosters wider collaboration and increased citations
- maximum visibility for your research: over 100M website views per year

**At BMC, research is always in progress.**

Learn more [biomedcentral.com/submissions](https://biomedcentral.com/submissions)

